Mitotic and Meiotic Functions for the SUMOylation Pathway in the *Caenorhabditis elegans* Germline

Rachel Reichman, Zhuoyue Shi, Robert Malone, and Sarit Smolikove[1]
Department of Biology, The University of Iowa, Iowa City, Iowa 52242
ORCID IDs: 0000-0003-4175-6843 (R.R.); 0000-0003-0062-3606 (S.S.)

ABSTRACT Meiosis is a highly regulated process, partly due to the need to break and then repair DNA as part of the meiotic program. Post-translational modifications are widely used during meiotic events to regulate steps such as protein complex formation, checkpoint activation, and protein attenuation. In this paper, we investigate how proteins that are obligatory components of the SUMO (small ubiquitin-like modifier) pathway, one such post-translational modification, affect the *Caenorhabditis elegans* germline. We show that UBC-9, the E2 conjugation enzyme, and the *C. elegans* homolog of SUMO, SMO-1, localize to germline nuclei throughout prophase I. Mutant analysis of *smo-1* and *ubc-9* revealed increased recombination intermediates throughout the germline, originating during the mitotic divisions. SUMOylation mutants also showed late meiotic defects including defects in the restructuring of oocyte bivalents and endomitotic oocytes. Increased rates of noninterfering crossovers were observed in *ubc-9* heterozygotes, even though interfering crossovers were unaffected. We have also identified a physical interaction between UBC-9 and DNA repair protein MRE-11. *ubc-9* and *mre-11* null mutants exhibited similar phenotypes at germline mitotic nuclei and were synthetically sick. These phenotypes and genetic interactions were specific to MRE-11 null mutants as opposed to RAD-50 or resection-defective MRE-11. We propose that the SUMOylation pathway acts redundantly with MRE-11, and in this process MRE-11 likely plays a structural role.

KEYWORDS meiosis; SUMOylation; DNA damage repair; germline; *ubc-9*

THE *Caenorhabditis elegans* germline is a dynamic organ that contains both mitotically dividing nuclei and nuclei undergoing meiosis (Hubbard 2005). The distal tip of hermaphroditic gonads contains mitotic nuclei that transition into meiosis, the process by which eggs and sperm are formed. Meiosis involves two rounds of cellular division; the first is reductional and the second equational. Meiosis initiates when homologous chromosomes pair and the synaptonemal complex (SC), a proteinaceous zipper-like structure, forms to hold homologs together (Dernburg *et al.* 1998; Plug *et al.* 1998; Walker and Hawley 2000). At this early stage of meiosis, SPO-11 forms DNA double-stranded breaks (DSBs) as the first step in homologous recombination (HR) (Klapholz *et al.* 1985; Cao *et al.* 1990; Malone *et al.* 1991; Keeney *et al.* 1997; McKim and Hayashi-Hagihara 1998; Romanienko and Camerini-Otero 1999). These DSBs are initially processed by the MRE11, RAD50, and NBS1/Xrs2 (MRN/X) complex. RAD-50's coiled-coil and hook domains hold the broken ends together, while MRE11 binds DNA, nicks the DNA upstream of SPO11, and resects the DNA leaving a short 3' overhang (Usui *et al.* 1998; de Jager *et al.* 2001; Borde *et al.* 2004; Milman *et al.* 2009; Hohl *et al.* 2011). The latter activity of the MRN/X complex removes SPO11 bound to the 5' end of the DNA and is required for long-range resection performed by other nucleases. The single-stranded binding protein RPA initially covers the single-stranded DNA (ssDNA), and then is replaced by the recombinase RAD51 and/or its meiosis-specific ortholog DMC1 (Bishop *et al.* 1992; Shinohara *et al.* 1992; Bishop 1994; Habu *et al.* 1996; Dresser *et al.* 1997; Yoshida *et al.* 1998). MSH4/5 then localizes to sites that will become interfering crossovers along with other crossover-promoting proteins, including COSA-1 in worms (Hollingsworth *et al.* 1995; Paquis-Flucklinger *et al.* 1997; Bocker *et al.* 1999; Novak *et al.* 2001; Snowden *et al.* 2004; Yokoo *et al.* 2012). Following crossover formation, chromosomes restructure, while the SC disassembles. Chiasmata

doi: https://doi.org/10.1534/genetics.118.300787
Manuscript received October 25, 2017; accepted for publication February 19, 2018; published Early Online February 22, 2018.
Available freely online through the author-supported open access option.
Supplemental material is available online at www.genetics.org/lookup/suppl/doi:10.1534/genetics.118.300787/-/DC1.
[1]Corresponding author: Department of Biology, Biology Building, The University of Iowa, Iowa City, IA 52242. E-mail: sarit-smolikove@uiowa.edu

(the physical manifestation of crossovers) hold the chromosomes together through the end of diakinesis (Rasmussen and Holm 1984; Lawrie *et al.* 1995; Moens and Spyropoulos 1995; Bascom-Slack *et al.* 1997).

Although the function of many meiotic proteins is understood, the complex regulation of HR is still under investigation. Many of the canonical HR proteins are modified post-translationally, by phosphorylation, ubiquitination, or SUMOylation (Falck *et al.* 2012; Lu *et al.* 2012; Bologna *et al.* 2015; Ismail *et al.* 2015; Parameswaran *et al.* 2015; Luo *et al.* 2016; Silva *et al.* 2016; Tomimatsu *et al.* 2017). SUMOylation is a modification that involves the transfer of a small polypeptide called small ubiquitin-like modifier (SUMO) to a target protein (Choudhury and Li 1997; Lapenta *et al.* 1997; Mahajan *et al.* 1997; Chen *et al.* 1998; Huang *et al.* 1998; Tanaka *et al.* 1999). Yeast and *C. elegans* have a single SUMO moiety, while mammals have three SUMO isoforms (Su and Li 2002). SUMOylation is used to modify protein function; it can be used to stabilize protein complexes, localize target proteins to specific cell organelles, or signal for degradation (similar to ubiquitination). The SUMOylation pathway consists of an E1 activating enzyme that binds SUMO (Haas *et al.* 1982). E1 then transfers SUMO to an E2 conjugating enzyme, which can transfer SUMO directly to a target protein (Bernier-Villamor *et al.* 2002). Alternatively, E2 can transfer SUMO to an E3 ligase that then SUMOylates the target protein (Yunus and Lima 2009). *C. elegans* uses the E1 enzymes UBA-2 and AOS-1, a single E2 enzyme UBC-9, and two canonical E3 ligases GEI-17 and ZK1248.11 (Holway *et al.* 2006; Pelisch and Hay 2016). A target protein can be monoSUMOylated, or polySUMOylated (Rojas-Fernandez *et al.* 2014; Horigome *et al.* 2016). The latter can be branched or straight depending on context. SUMO chains can help create larger structures that may hold macromolecules together *in vivo* (Tatham *et al.* 2001; Bylebyl *et al.* 2003; Windecker and Ulrich 2008; Skilton *et al.* 2009; Guzzo *et al.* 2012; Rojas-Fernandez *et al.* 2014; Chen *et al.* 2016). SUMOylation is a regulated process, and SUMO can be added to or removed from target proteins depending on cellular input. SUMO moieties that are conjugated to target proteins can then interact noncovalently with other proteins' SUMO-interacting motifs (SIMs) to form functional complexes (Song *et al.* 2004).

Evidence that SUMOylation is required for proper meiosis has been found from studies in *Saccharomyces cerevisiae* and mice (Voelkel-Meiman *et al.* 2013; Chen *et al.* 2016). In yeast, immunofluorescence reveals that both UBC9 (E2) and SUMO localize to the SC during early prophase I, and that deletion of either protein prevents normal SC assembly (Hooker and Roeder 2006; Voelkel-Meiman *et al.* 2013). UBC9 interacts with proteins that act in meiotic recombination in mammals and yeast, in a step required for RAD-51 filament assembly. RNF212 is an E3 SUMO ligase that has been shown to regulate meiotic recombination in mice (Rao *et al.* 2017). RNF212 acts by stabilizing recombination sites through controlling HEI10-mediated proteasomal degradation of proteins promoting noncrossover pathways. RAD51 and UBC9 colocalize during spermatogenesis in mice (Kovalenko *et al.* 1996). In yeast, Rad52 and Rad59 are both SUMOylated; this is required for Rad52 stabilization and for Rad52/Rad59 function in loading Rad51 onto ssDNA (Sacher *et al.* 2006; Altmannova *et al.* 2010).

SUMOylation in mitosis has been examined in many organisms including yeast and mammals. In mammals, three SUMO paralogs with distinct but overlapping functions are expressed (Citro and Chiocca 2013). SUMO1 is important for all the major pathways of DSB repair, and the other two paralogs, SUMO2 and SUMO3, are required for classic nonhomologous end joining (Hu and Parvin 2014). In mammalian tissue culture, RNF4 forms SUMO/ubiquitin hybrid chains through its SIM domain and is required for localization of BRCA1 and RAP80 to DNA damage foci (Guzzo *et al.* 2012). RNF4 also recognizes polySUMOylated proteins including RPA, BRCA1, 53BP1, and MDC1 *in vivo*, and is responsible for targeting them for degradation via the ubiquitin pathway (Galanty *et al.* 2012; Yin *et al.* 2012; Vyas *et al.* 2013). RNF4 in mammals responds to replication stress, as it is localized at stalled replication forks when ATR is depleted (Ragland *et al.* 2013). Rad52/Rad59 are also targets for SUMOylation in mitosis, where they plays a role in repair pathway choice (Silva *et al.* 2016). In yeast mitosis, Rad52/Rad59 SUMOylation regulates Srs2, which itself is SUMOylated. All three SUMOylated proteins affect the crossover *vss*. gene conversion decision in HR as well as the choice between the single-strand annealing pathway and HR. This pathway choice could be mediated by the Rad52/59 complex role in Rad51 loading (Altmannova *et al.* 2010; Silva *et al.* 2016). Rad52/Rad59 is not the only target of SUMOylation in DNA repair. Studies in yeast have demonstrated that both Mre11 and Xrs2 of the MRX complex are SUMOylated upon DNA damage (Cremona *et al.* 2012; Sarangi *et al.* 2015). Mre11 in yeast uses SIMs to associate with SUMO on other proteins (Chen *et al.* 2016). SIMs may help hold the complex together in a structurally functional conformation.

SUMOylation has been most extensively studied in the *C. elegans* soma in the context of development. UBC-9 and/or SUMO play a role in vulva development, telomere localization, dosage compensation, pharynx development, ER stress response, adherens junction and cytoplasmic intermediate filament assembly, nuclear localization of FIGL-1, and in targeting sensory receptors in primary cilia (Broday *et al.* 2004; Leight *et al.* 2005; Roy Chowdhuri *et al.* 2006; Kaminsky *et al.* 2009; Li *et al.* 2012; Ferreira *et al.* 2013; Pferdehirt and Meyer 2013; Ward *et al.* 2013; Lim *et al.* 2014; Tsur *et al.* 2015). In the germline, the SUMO pathway was examined by the analysis of *smo-1(ok359)* null mutants and was reported not to be required for crossover formation, but led to SC disassembly defects (Bhalla *et al.* 2008). Depleting *ubc-9* via RNAi (RNA interference) confers a radiation-sensitive phenotype in *C. elegans* (Boulton *et al.* 2004). UBC-9 has also been shown to physically interact with RAD-51, BRC-1, and BRD-1, a functional partner of BRC-1, through yeast

two-hybrid and *in vitro* pull-down assays (Boulton *et al.* 2004). Despite these physical interactions with UBC-9, assays were unable to detect direct interactions between the SUMO moiety and RAD-51 or BRC-1 (Boulton *et al.* 2004).

In this paper, we demonstrate that SUMOylation is important for proper *C. elegans* germline function, with both premeiotic replication and meiosis negatively affected when SUMO-1 or UBC-9 function is abrogated. We find that DNA breaks are increased in mitotically dividing nuclei in the premeiotic tip (PMT) and fail to repair before transitioning into meiosis. Prophase I nuclei have meiotic progression defects and show an increase in recombination intermediates. Oocytes in SUMOylation mutants fail to properly form in both *smo-1* and *ubc-9* null mutants, resulting in sterility. Multiple germline defects in SUMO pathway mutants indicate potential roles for SUMO in the DNA damage repair (DDR) in response to replication fork collapse in the PMT and roles in meiotic HR.

Materials and Methods

Strains

All strains were cultured at 20° on plates containing OP50. N2 worms were used as the control strain for all experiments (Brenner 1974). All mutant alleles and transgenic lines used were outcrossed six times into the N2 background. Wild-type Hawaiian line CB4856 hermaphrodites were used for SNP recombination mapping and crossed to ubc-9(*tm2610*)/nT1 males (Swan *et al.* 2002). The nT1 balancer is a reciprocal translocation of chromosomes VI and V, and homozygous balancer progeny are lethal (Edgley *et al.* 2006). Mutant lines and transgenic lines used were: *ubc-9(tm2610)*, *spo-11(ok79)*, *mre-11(iow1)*, *mre-11(ok179)*, *smo-1(ok359)*, *fgpIs20 [(pAA64) pie-1p*::*mCherry*::*smo-1(GG) + unc-119(+)*, *fgpIs21 [(pAA64) pie-1p*::*mCherry*::*smo-1(GA) + unc-119(+)]*, *meIs8 [pie-1p*::*gfp*::*cosa-1 + unc-119(+)]II*, *ubc-9(iow31[3xflag*::*ubc-9])IV/nT1[qIs51] (IV;V)*, and *mre-11(iow45[mre-11*::*gfp])*.

Yeast two-hybrid

Two *C. elegans mre-11* cDNA fragments were cloned into the pLexA gateway vector (plasmid #11345; Addgene) and pACT2.2. The *C. elegans* yeast two-hybrid library was generated by Guy Caldwell (University of Alabama) and obtained from Addgene (plasmid # 11523). The *mre-11* C-terminal truncation contained the first 1263 bp of cDNA encoding the first 421 amino acids of MRE-11. The *mre-11* N-terminal truncation contained 1021 bp of cDNA encoding the last 339 amino acids. Putative interactions were detected through screening for histidine reporter gene expression and further validated via X-gal (5-bromo-4-chloro-3-indolyl-beta-D-galactopyranoside) assays. Colonies with strong growth in the absence of histidine and blue color when incubated with X-gal were sequenced. For *ubc-9/mre-11* interaction validation, a full-length *mre-11* cDNA was cloned, and a targeted yeast two-hybrid assay was conducted between full-length and both N- and C-terminal truncations of MRE-11 coupled with full-length UBC-9 cloned into the pAct2.2 gateway vector (plasmid # 11346; Addgene). Interactions were detected through X-gal assay expression (Supplemental Material, Figure S1 in File S1).

Clustered regularly interspaced short palindromic repeats (CRISPR)/CAS9 generation of mre-11::gfp, 3Xflag::ubc-9 and rad-51::3Xflag lines

The *gfp* repair template was cloned into the pDD282 C-terminal gfp plasmid with a hygromycin cassette (Dickinson and Goldstein 2016). On either side of the break, > 500-bp homology arms were cloned via PCR. The single-guide RNA (sgRNA) sequence used for *mre-11*::*gfp* was 5′-GTTCTCGAAGTAGAC TGTGG-AGG-3′. Silent mutations at the protospacer adjacent motif (PAM) site of the repair template were introduced to prevent cutting after gfp integration, per the standard protocol. The *3Xflag*::*ubc-9* repair template used was a 200-bp single-stranded oligodeoxynucleotides (ssODN) ordered from Integrated DNA Technologies. The ssODN sequence was: 5′-ccacttctcttttacaaatttgatatttttcagtgtaaccgaacaaaaATGgactacaa agaccatgacggtgattataaagatcatgaTatcgaTtacaaggatgacgatgac aagTCGGGAATTGCTGCAGGACGCCTCGCTGAGGAGAGAAA ACACTGGCGAAAGgtgagaattttatcattacatggcaagtcggg-3′. Lowercase letters after the ATG indicate the 3Xflag sequence [uppercase letters indicate silent mutations made in the 3Xflag sequence to create *Eco*RV and *Cla*I sites, as referenced in Paix and Wang (2014)]. sgRNA was cloned into the pIK198 vector (Katic *et al.* 2015). pIK198 was generated by Iskra Katic (plasmid # 65629; Addgene). The sgRNA sequence used is 5′-CAGGACGCCTCGCGGAAGAA-AGG-3′. The PAM site sequences are provided after the dash for reference. 3Xflag insertion can be detected in a 2% agarose gel run at 105 V for 1.5 hr after PCR using primers F: 5′-CTGACAAGTGTCAC GAACACG-3′ and R: 5′-CGGGAAATCGTCCTTGAAGAG-3′ at 55.3° for 40 sec. Wild-type size: 591- bp PCR product; flag insertion size: 655- bp PCR product. *3Xflag*::*ubc-9* worms are balanced with nT1 because of developmental problems resulting in larval lethality in homozygous offspring. *3Xflag*::*ubc-9* homozygotes or *ubc-9(tm2610) /3Xflag*::*ubc-9* are viable and develop normal gonads (as determined by DAPI morphology, synapsis, bivalent formation, and RAD-51 kinetics), but *3Xflag*::*ubc-9* or *ubc-9(tm2610) /3Xflag*::*ubc-9* produce no viable progeny, indicating that *3Xflag*::*ubc-9* creates a protein that is functional in the germline but not in early embryonic development. Since *3Xflag*::*ubc-9* still functions normally in the germline, anti-FLAG staining can be used to examine the UBC-9 pattern of localization. The *rad-51*::*3Xflag* line was created by using an ssODN repair template to insert the 3Xflag sequence just prior to the stop codon. The ssODN sequence is: 5′-CAATCACGAATCATGG TATTGAGGACGCACGCGAAGACgactacaaagaccatgacggtgatta taaagatcatgaTatcgaTtacaaggatgacgatgacaagTAGccgttcgtttttct ttttcttatcaaacttca-3′. ssODN was injected with a C-termina sgRNA, 5′-TGGTATTGAGGACGCACGCG-3′, and recombinant Cas9 protein (University of California, Berkeley), along with

the *dpy-10* co-injection marker. Injections were performed on *ubc-9(tm2610)/nT1(GFP)* hermaphrodites. GFP^+ F1 offspring that were dumpy or rollers were singled and then insertions were screened via PCR after 3 days. Primers used for screening were F: 5′-GAAGCCGAAGCGACCTACTCA-3′ and R: 5′-CATGAGGGGCAGGCG-3′, used at 62° with an extension time of 20 sec. A 2% gel was used to separate bands, with wild-type = 225 bp and FLAG insertion = 300 bp. A heterozygote line was established and GFP^- worms were screened to determine whether the FLAG tag was on the nonbalancer chromosome. Sequencing determined whether the tag was in frame.

Immunostaining and microscopy

Gonads were dissected and immunostained as described in Colaiacovo *et al.* (2003). Both whole worms and dissected gonads were prepared 20-hr post-L4. Antibodies used were as follows: rabbit anti-RAD-51 (1:10,000; ModEncode), preabsorbed mouse anti-SMO-1 (1:10 Developmental Studies Hybridoma Bank 6F2), mouse anti-FLAG (1:100; Sigma [Sigma Chemical], St. Louis, MO), rabbit anti-phospho histone 3 (PH3) (1:5000; Upstate Biotechnologies), and rabbit anti-SUN-1 (1:5000; Sdix). Secondary antibodies used were Alexa Fluor 488-anti-rabbit antibody (1:500) and Alexa Fluor 550-anti-mouse antibody (1:500). Whole worms were ethanol-fixed for COSA-1:GFP imaging and stained with DAPI [1:2000 dilution of a 5-mg/ml DAPI stock in PBS tween (PBST)] and mounted with Vectashield mounting medium. *syp-3*::*gfp*, *mCherry*::*smo-1* lines and *mre-11:gfp* worms were dissected, frozen on dry ice blocks, fixed for 15 min in 4% paraformaldehyde in the dark, then washed with PBST for 5 min, stained with DAPI for 10 min, and washed in PBST for 10 min. Slides were mounted with Vectashield.

Images were taken with a DeltaVision wide-field fluorescence microscope system (Applied Precision) with an Olympus 100×/1.40-numerical aperture lenses. Optical sections were collected at 0.20-μm increments with a $coolSNAP_{HQ}$ camera (Photometrics) and softWoRx software (Applied Precision), and deconvolved using softWoRx 5.0.0 software. Images are projections through three-dimensional data stacks of whole nuclei (15–30 0.2-mm slices/stack).

Focus quantification

RAD-51 focus quantification was performed at four stages: PMT, the transition zone (TZ) that includes leptotene and zygotene, early pachytene (EP), and mid/late pachytene (MLP). Nuclear morphology (DAPI staining) and SYP-1 antibody staining were used to identify the four stages in the germline (Yin and Smolikove 2013). GFP::COSA-1 foci were counted in zone 7 in late pachytene, before diplotene.

Mitotic index calculation

At least 10 gonads were analyzed per genotype to calculate the average mitotic index (MI). PH3 staining marks metaphase nuclei in the PMT. The ratio of stained nuclei/total PMT nuclei was calculated as the MI.

Length and width gonad measurements

Whole worms were ethanol-fixed and stained with DAPI, then mounted with Vectashield. Images were taken at 10× magnification. Gonad length was measured in ImageJ. Length measurement was defined as the distance from the beginning of the PMT to the beginning of diplotene. Width measurements were taken at two points: the 50% mark in the PMT and the 50% mark from the TZ to the end of pachytene. The genotypes measured were not significantly different in overall body size.

EMO phenotype measurements

Whole worms were fixed with ethanol and stained with DAPI. Worms were mounted with Vectashield. A minimum of 10 gonads was analyzed for each genotype. Endomitotic oocyte (EMO) was defined as prematurely replicating nuclei that did not display bivalents but instead produced a single decondensed mass of DNA (Iwasaki *et al.* 1996). The number of endomitoic (Cremona *et al.* 2012) diakinesis oocytes were counted and divided by the total number of diakinesis oocytes in the germline.

UBC-9/SUN-1 colocalization measurements

Fifteen nuclei were measured in total from three different gonads that were stained for FLAG:UBC-9 and SUN-1 and DAPI. Two intensity peaks were measured per nucleus for each protein for 15 nuclei measured. Images were analyzed in FIJI using the Plot profile function. Z-stacks were used to determine the approximate halfway point through the nucleus, and then a line was drawn through both walls of the nuclear envelope. The plot profile data was then downloaded into Excel (Microsoft, Redmond, WA) for all three channels, and intensity peaks were determined for SUN-1 and UBC-9. Positive or negative values were determined based on whether the UBC-9 peak was inside or outside of the SUN-1 peak relative to the center of the nucleus. If UBC-9's peak signal was outside of the SUN-1 peak relative to the center of the nucleus, the measurement was negative. If UBC-9's peak fell inside of the SUN-1 peak relative to the center of the nucleus, then the measurement was positive.

Camptothecin/hydroxyurea adult assay

aaSeeded OP50 worm plates were exposed to UV light for 1 hr (placed on a UV illuminator from Fisher) to kill the bacteria so to prevent the metabolism of the camptothecin (CPT) or hydroxyurea (HU). Then, a final concentration of either 5.25 mM HU diluted in M9 or 350 nM CPT (10 mM stock CPT diluted in DMSO, final concentration diluted in M9 pH6) was plated and allowed to soak in overnight in the dark. One day post-L4 worms of each genotype were placed on the treated plates for up to 8 hr in 2 hr increments in the dark. Control worms were dissected immediately without being exposed to any chemicals. Worms were promptly dissected according to normal protocols and stained with RAD-51

antibody (1:10,000). Three to nine gonads were counted for each genotype and treatment.

Larval lethality assay

A single heterozygote L4 worm of the nT1 balancer was added per plate with a small lawn of spread OP50 (1 cm^2) that was grown overnight at room temperature. The worm was transferred to a new plate every 24 hr for 4 days. Eggs were counted after 24 hr, and larvae and adults were counted for a total of 6 days after egg lay to account for delayed development. Both GFP^+ and GFP^- worms were counted under a GFP dissection scope to collect data from heterozygote (GFP^+) and homozygote (GFP^-) mutant offspring.

Recombination frequency mapping

ubc-9(tm2610)/nT1 males in the N2 background were crossed to CB4856 hermaphrodites to create *ubc-9(tm2610)*/+ heterozygotes with N2/CB4856 SNP distribution. Twelve GFP^- F1 L4 hermaphrodites were moved to individual plates and let lay for 3 days. Eight F2 offspring were lysed from each of the 12 F1's for a total of 96 offspring per cross that were analyzed. The F1 worms were also lysed and analyzed for SNP heterozygosity. Two SNPs were analyzed on chromosome II at location −18 and 11 using *Dra*1 digestion. At location −18, N2: 263 + 112 bp PCR product; CB4856: 375 bp PCR product. At location 11, N2: 483 bp PCR product; CB4856: 352 + 132 bp PCR product. N2 and CB4856 lines were used as controls to ensure complete *Dra*I (New England Biolabs, Beverly, MA) digestion. The formula used to calculate the recombination frequency is $p = 1-(1-R)^{1/2}$. R = [(number of animals heterozygous for one marker and homozygous for the other) + 2 × (number of animals homozygous for recombinant chromosomes)]/total number of animals scored (Brenner 1974; Bazan and Hillers 2011).

Data availability

Strains are available upon request. The authors state that all data necessary for confirming the conclusions presented in the article are represented fully within the article.

Results

MRE-11 and UBC-9 physically interact in a yeast two-hybrid assay

To better understand how MRE-11 is regulated in meiosis, we aimed to identify proteins physically interacting with *C. elegans* MRE-11. We conducted a yeast two-hybrid screen using C-terminal and N-terminal fragments of MRE-11 as the bait. UBC-9 was identified as an interacting protein; the yeast two-hybrid interaction was also found with full-length MRE-11 (Figure S1 in File S1). *ubc-9* encodes the SUMO E2 conjugating enzyme.

UBC-9 and SMO-1 localize to the nuclear periphery in the C. elegans germline

MRE-11 is a protein required for meiotic recombination in *C. elegans*, as found in other organisms (Chin and Villeneuve 2001; Goodyer *et al.* 2008). If UBC-9 interacts with MRE-11 *in vivo*, they should both be expressed in the same tissue. Previous studies have indicated that both SUMO-1 and UBC-9 are expressed in the germline, but it was not clear in which stage of meiotic prophase I they were expressed (Pelisch *et al.* 2014,,2017). We created a *3Xflag*-tagged *ubc-9* line via CRISPR/Cas9 homology recombination repair (Figure 1, A and B). The *3Xflag* tag was inserted at the N-terminus of *ubc-9* directly following the ATG start codon. *flag*::*ubc-9* worms have normal gonad morphology and RAD-51 staining, but do not produce viable progeny, indicating that the FLAG::UBC-9 protein is dysfunctional only for processes required for development after oocyte formation (*Materials and Methods* and Figure S2A in File S1). Anti-FLAG immunostaining of *3Xflag*::*ubc-9* homozygotes shows that UBC-9 localizes to nuclei in the PMT through late pachytene in a punctate pattern with an enrichment near the nuclear membrane (Figure 1A). FLAG staining was not observed in wild-type worms that do not contain the flag tag (Figure S2B in File S1). UBC-9 was absent from diplotene and diakinesis nuclei (data not shown).

To observe where in the *C. elegans* gonad the SUMO protein, SMO-1, localizes, we used an antibody for SMO-1 and found a diffuse nuclear localization pattern (Figure 1C and Figure S2C in File S1). To test for specificity of staining we analyzed two mutants: *ubc-9(tm2610)*, a 315- bp deletion mutant that encompasses the region encoding the SUMO-binding site in UBC-9, and *smo-1(ok359)*, a complete deletion of the only *C. elegans* SUMO gene. The *smo-1* gene is essential, but *smo-1(ok359)* homozygous progeny produced from balanced hermaphrodites are viable and reach adulthood likely due to maternally provided SMO-1 (Broday *et al.* 2004). SMO-1 nuclear staining was specific, as both *smo-1(ok359)* and *ubc-9(tm2610)* null mutants lacked nuclear staining. We also utilized two transgenic lines containing an mCherry::SUMO-1 fusion transgene with a wild-type endogenous *smo-1* gene generated by bombardment (Pelisch *et al.* 2014). One transgenic line contained a wild-type *smo-1* gene [SMO-1(GG)], whereas the other had a point mutation allele for the last amino acid, rendering the SMO-1 protein unconjugatable [SMO-1(GA)]. SMO-1(GG) showed nuclear localization using the anti-SUMO antibody, similar to what we observed with the antibody staining for wild-type strains (Figure 1D). The mutant form SMO-1(GA) showed cytoplasmic, but not nuclear, localization in a filament-like pattern. (Figure 1D). In a *ubc-9(tm2610)* mutant background, neither the wild-type [SMO-1(GG)] nor the unconjugatable form [SMO-1(GA)] localized to the nucleus (Figure 1D). Only if the SUMO E2 enzyme and conjugatable SUMO are present can SUMO be found in the nucleus. We therefore presume that SUMO and UBC-9 modify a germline nuclear target(s).

The localization pattern of 3XFLAG::UBC-9 is enriched at the nuclear envelope, but anti-FLAG staining alone did not identify whether UBC-9 was inside or outside of the nuclear envelope. We costained with a SUN-1 antibody (that marks the inner nuclear membrane) and a FLAG antibody to identify

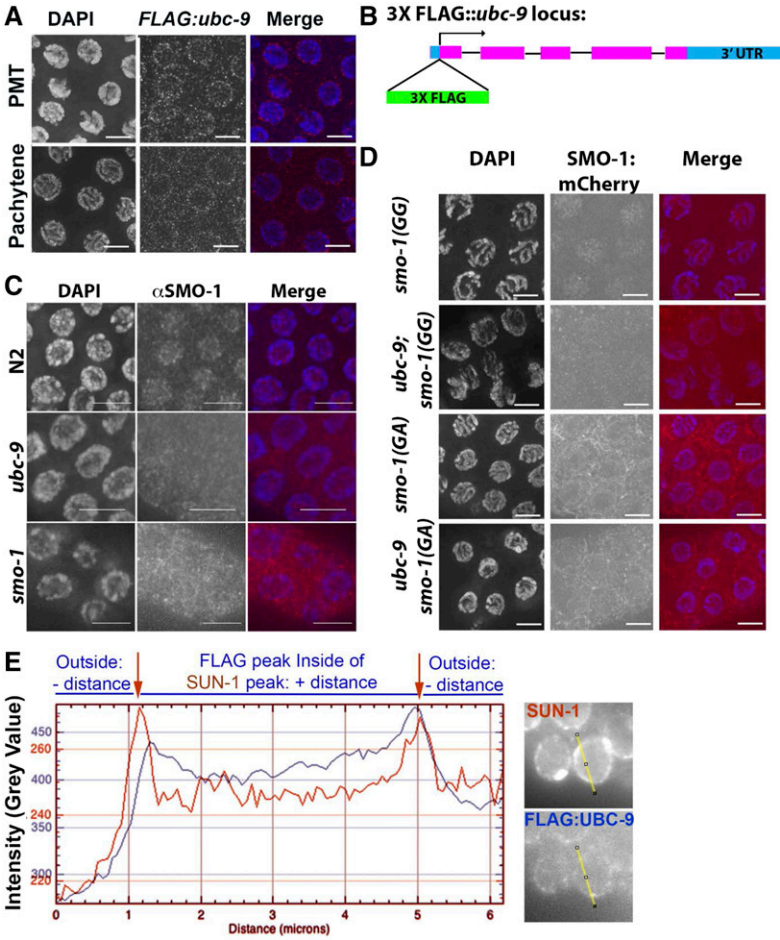

Figure 1 UBC-9 and SMO-1 localize to the nucleus in the *C. elegans* germline. (A) 3XFLAG::UBC-9 localizes to the nuclear periphery throughout the germline in the wild-type (WT) strain. Premeiotic tip (PMT) and mid/late pachytene are shown. DAPI is blue, 3XFLAG::UBC-9 is red. (B) Schematic of *3Xflag* insertion in the N-terminus of the endogenous *ubc-9* locus. The tag is inserted directly after the start codon. (C) Endogenous SMO-1 localization in WT, *ubc-9(tm2610)*, and *smo-1(ok359)* strains. Nuclear localization is present in WT, but in *ubc-9* mutants staining is diffuse with no nuclear preference. *smo-1* mutants have low levels of background staining with no nuclear enrichment. DAPI is blue, SMO-1 is red. (D) smo-1::mCherry lines with a WT sequence (GG), or a nonconjugatable point mutation (GA), were expressed in WT and *ubc-9* backgrounds. Nuclear mCherry expression is visible in the WT *smo-1(GG)* strain, but not when *ubc-9* is mutated. *smo-1(GA)* strains have diffuse cytosolic staining in both WT and *ubc-9* mutants. All images are midpachytene stage. (E) Graph of signal intensity peaks. Representative lines used for analysis taken 50% through the nucleus for SUN-1 and 3XFLAG::UBC-9 are shown.

whether UBC-9 localizes close to the nuclear membrane (Figure 1D and Figure S2D in File S1) (Tzur *et al.* 2006; Penkner *et al.* 2007; Minn *et al.* 2009). Figure 1D and Figure S2D in File S1 indicate that the positions of UBC-9 and SUN-1 are not significantly different, confirming that UBC-9 is associated with the nuclear membrane. Our data suggest that UBC-9 may in fact be located on the inner membrane (Figure 1D).

Gonads in SUMOylation mutants are smaller than wild-type

Both *smo-1(ok359)* and *ubc-9(tm2610)* mutant worms are completely sterile and do not lay eggs. Their protruding vulva phenotype could potentially explain the lack of egg laying (Horvitz and Sternberg 1991; Greenwald 1997; Broday *et al.* 2004). However, defects in germline development could also contribute to the sterility observed. In the nematode *C. elegans* germline, prophase I occurs along the germline in spatiotemporal organization; the syncytial germline nuclei are generated at the distal tip and then flow toward the proximal end of the gonad as nuclei progress through meiosis. Examination of *ubc-9(tm2610)* and *smo-1(ok359)* mutant germlines via DAPI staining revealed that these mutants contain a germline with most stages of meiosis with several defects (discussed in detail below). Gonads of *ubc-9(tm2610)* and *smo-1(ok359)* homozygotes were 33.1 and 36.4% shorter in length and 33.4 and 59.6% smaller in width at midpachytene, respectively, compared to wild-type (Figure S3 in File S1 and Tables S1 and S2 in File S3).

DSBs are increased in SUMOylation pathway mutants and atypical RAD-51 foci are observed

The SC assembled without any observable defects in both *ubc-9(tm2610)* and *smo-1(ok359)* mutants. This is in agreement with a previous study describing no SC assembly defect in *smo-1(ok359)* mutants (Bhalla *et al.* 2008) and with the lack of SC-specific localization of UBC-9 and SMO-1 in *C. elegans* (this study). Wild-type nuclear SMO-1 localization, coupled with reduced germline size without SC phenotypes in SUMOylation mutants, suggests that the SUMO pathway in *C. elegans* may be involved in other aspects of germline function such as DNA repair in the PMT and/or meiotic recombination. A role in these pathways is suggested by the physical interaction found between UBC-9 and MRE-11 in the yeast two-hybrid assay.

C. elegans lacks a DMC1 homolog; therefore RAD-51 is the only recombinase present in meiosis (Takanami *et al.* 1998). We dissected gonads to stain for RAD-51, which measures the number of ssDNA recombination intermediates to which RAD-51 can bind (Figure 2,Figure S4 in File S1, and Tables S3 and S4 in File S3). RAD-51 is essential for HR (Shinohara

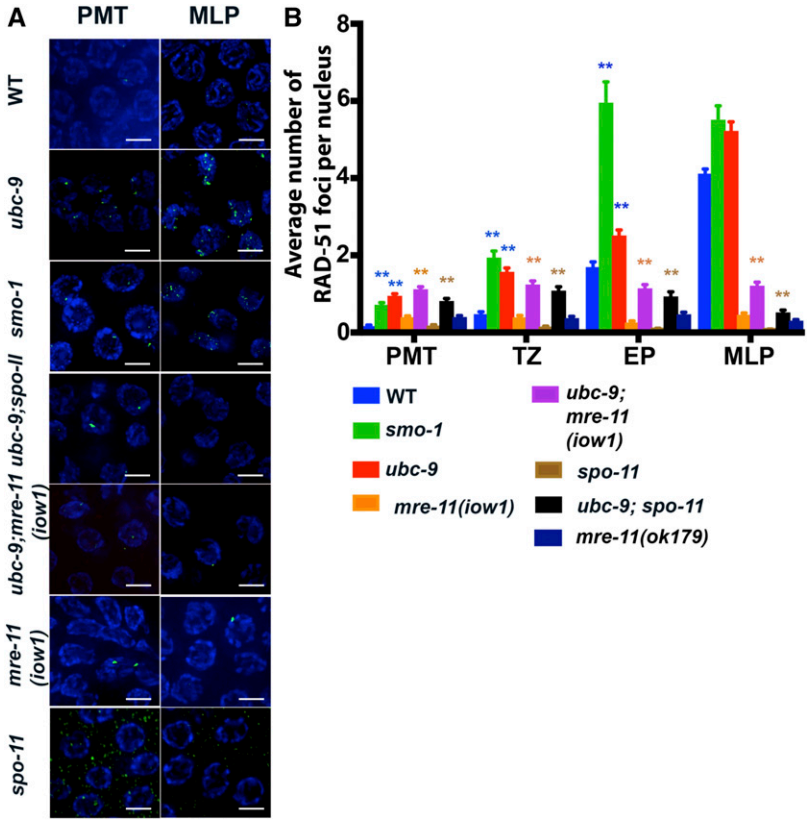

Figure 2 RAD-51 foci numbers are increased in SUMOylation mutants. (A) Representative images of RAD-51 foci from the premeiotic tip (PMT) and mid/late pachytene (MLP) of wild-type (WT) and mutants. RAD-51 is green, DAPI is blue. (B) RAD-51 foci data count each type of aberrant RAD-51 focus (singlet, doublet, triplet, quadruplet, and string) as one focus. The colors of significance stars are what each mutant is compared to [*i.e.*, *ubc-9(tm2610)* has blue stars above it because it is being compared to WT (blue bar)]. Full pairwise comparison charts with significance are found in the supplements. Error bars signify the mean ± SEM. Three full gonads were counted per genotype except *ubc-9(tm2610)* single mutants where five full gonads were counted. *n*-values: PMT range from 236 to 667 nuclei counted per genotype, transition zone (TZ) range from 129 to 268 nuclei counted, early pachytene (EP) range from 69 to 271 nuclei counted, and MLP range from 199 to 660 nuclei counted.

et al. 1992). The presence of wild-type SC in *ubc-9(tm2610)* and *smo-1(ok359)* mutants allows the precise staging of meiotic nuclei based on SC morphology (see below) (Yin *et al.* 2016). SYP-1 antibody was used to place germline nuclei into four stages: the PMT that lacks SYP-1 staining, the TZ that has SYP-1 puncta, EP that contain regions of linear SYP-1 that are not full-length, and MLP that contains fully linearized SYP-1 along the entire chromosome. RAD-51 foci were increased in the PMT in both *ubc-9(tm2610)* and *smo-1(ok359)* mutants (0.16 ± 0.02 foci/nucleus in wild-type to 0.95 ± 0.05 and 0.71 ± 0.06 foci on average, respectively, Figure 2). This indicates that SUMOylation plays a role in the PMT and that a lack of SUMO leads to increased ssDNA loaded with RAD-51. RAD-51 foci in the PMT could be generated by collapsed replication forks. A similar increase is also observed in TZ (wild-type 0.48 ± 0.06, *ubc-9(tm2610)* 1.57 ± 0.1, and *smo-1(ok359)* 1.94 ± 0.17 foci/nucleus) and EP nuclei (wild-type 1.7 ± 0.13, *ubc-9(tm2610)* 2.51 ± 0.14, and *smo-1(ok359)* 5.95 ± 0.54 foci/nucleus). Foci also are seen in both diplotene and diakinesis in the SUMOylation mutants, but are absent from these stages in wild-type worms.

In addition to the increase in RAD-51 foci, atypical RAD-51 forms were observed in SUMOylation mutants. Wild-type RAD-51 foci primarily appear as single round dots, but we observed atypical RAD-51 foci that formed detectable doublets, triplets, quadruplets, and long string-like filaments in the two SUMOylation mutants (Figure 3 and Table S5 in File S3). Doublets, triplets, and quadruplets were categorized as two, three, or four foci, respectively that are clearly discernable but in contact with each other and have no space between them. We also observed strings: RAD-51 structures that are smooth, long structures that resemble filaments. Wild-type gonads had 8.1% doublets in the PMT and 0–10.2% atypical foci throughout meiotic nuclei (Figure 3B). Although both *ubc-9(tm2610)* and *smo-1(ok359)* mutants exhibit atypical RAD-51 structures in addition to normal foci, there are differences between the frequencies found in the two strains. In the PMT, 25.6% of foci are doublets in *ubc-9(tm2610)* mutants, whereas 18.1% of foci are doublets in *smo-1(ok359)* mutants. For triplets, quadruplets, and strings, both *ubc-9(tm2610)* and *smo-1(ok359)* mutants have roughly twice as many atypical forms as wild-type in almost all meiotic stages (Figure 3B and Figure S5 in File S1). The data in Figure 2 was generated for each form counted as 1 (*i.e.*, doublet, triplet, or quadruplet foci, or strings, were all counted as one focus). This is the standard technique for analyzing RAD-51 foci in the *C. elegans* germline (Yin and Smolikove 2013). We wondered whether counting of atypical foci as several foci would affect the outcome. We performed an alternative count of the same data counting each discernible part of an aberrant focus as one (Figure S4 in File S1). The conclusions from this method of counting were consistent with the ones drawn from Figure 2; *ubc-9* and *smo-1* mutants have increased levels of RAD-51 foci (see *Discussion*).

RAD-51 strings could be due to elevated DSBs in SUMOylation mutant backgrounds. To test this, we irradiated *ubc-9(tm2610)*

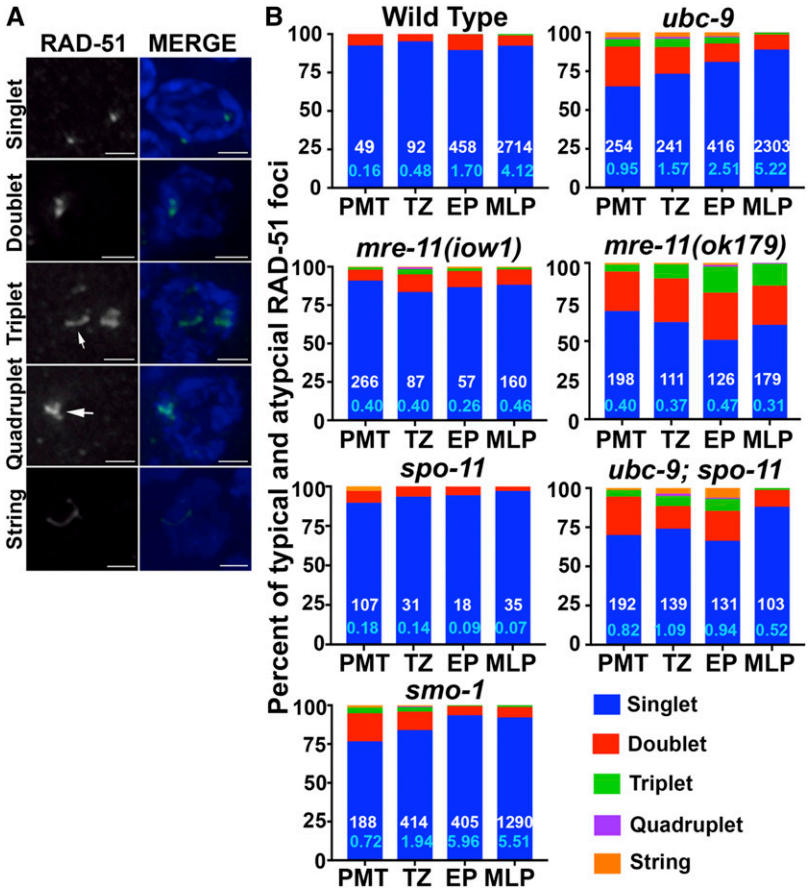

Figure 3 The fraction of alternate RAD-51 foci is increased in SUMOylation mutants and *mre-11* null mutants. (A) Representative images for each type of RAD-51 focus. The singlet picture is from a wild-type germline. Doublets, triplets, and quadruplet images were taken from *ubc-9(tm2610)* germlines and string image was taken from a *smo-1(ok359)* germline. Arrows point to the focus of interest. All images were taken from the premeiotic tip (PMT). (B) All graphs are percentage of total foci for the five RAD-51 categories. PMT, TZ (transition zone), EP (early pachytene), and MLP (mid/late pachytene). White numbers at the bottom of the blue bars indicate the total number of foci scored (both typical and atypical) included in that stage, while the light blue number is the average number of foci per stage and genotype.

and wild-type worms to create increased DSBs in the germline. There was no increase in the percentage of total nuclei with string-like structures, in either the wild-type or *ubc-9(tm2610)* mutant, compared to nonirradiated worms (Figure S5 in File S1 and Table S6 in File S3).

mre-11 mutants exhibit differences in aberrant RAD-51 focus patterns

Null *mre-11(ok179)* mutants have fewer RAD-51 foci in meiotic nuclei in all stages because they cannot make DSBs to initiate recombination. However, they do have a small increase in RAD-51 foci numbers in the PMT compared to wild-type (0.40 ± 0.03 compared to 0.17 ± 0.02 $P < 0.0001$); the latter is capable of forming DSBs but cannot process them, leading to low levels of RAD-51 foci throughout meiosis (Figure 2B). Furthermore, *mre-11(ok179)* mutants have a high percentage (25–30%) of RAD-51 doublets in all four germline stages, compared to doublets in both wild-type (5.4–10.3%) and *mre-11(iow1)* (7.1–11.5%) (Figure 3 and Table S5 in File S3).

In SUMOylation mutants, repair of recombination intermediates generated in mitosis is not completed before meiotic entry

Because both SUMOylation mutants exhibited an increase in RAD-51 foci in the PMT, we asked whether PMT foci were being carried over into meiosis. SPO-11 is the meiosis-specific protein required for the formation of meiotic DSBs. The numbers of RAD-51 foci in the PMT in *ubc-9(tm2610);spo-11(ok79)* double mutant was comparable to that *of ubc-9(tm2610)* mutants (Figure 2B). Similar numbers of RAD-51 were observed in meiotic zones (lower than found in *ubc-9* mutants and higher than in *spo-11(ok79)* single mutants). This data indicated that the elevated levels of RAD-51 foci in *ubc-9* mutants are caused by unrepaired DSBs carried over from mitosis to meiotic prophase.

Due to the increase in nuclear RAD-51 foci in SUMOylation mutants, we tested for a global increase in RAD-51 protein in *ubc-9(tm2610)* mutants compared to wild-type strains by performing a western blot for FLAG-tagged RAD-51 (Figure S6B in File S2). We generated a *rad-51*::*flag* line in the *ubc-9(tm2610)/nT1* background. Anti-FLAG staining showed RAD-51::FLAG foci that colocalized with antibody for RAD-51 (Figure S6B in File S2). Balanced and homozygous *ubc-9(tm2610)* strains had no detectable differences in the levels of RAD-51::FLAG protein, indicating that a loss of SUMOylation does not affect RAD-51 protein levels.

A synthetic sick interaction between ubc-9 and mre-11 null mutations

In *C. elegans* meiosis, MRE-11 is required both for DSB formation and for subsequent resection; both of these activities are absent in the null *mre-11(ok179)* mutant. Deleting *mre-11* in the *ubc-9(tm2610)* background caused developmental

and germline defects that were more severe than the ones observed in *ubc-9(tm2610)* single mutants (Figure 4 and Table S7 in File S3). nT1 is a balancer translocation chromosome that covers both *ubc-9* and *mre-11* on chromosomes IV and V, respectively (Edgley *et al.* 2006). nT1 is lethal when homozygous. A +/nT1 strain produced 24.3% homozygous wild-type larvae. A *ubc-9*/nT1 strain produced less (17.3%) homozygous *ubc-9* progeny ($P = 0.0012$, Fisher's exact test). Homozygous *ubc-9(tm2610)* progeny were also less likely to reach adulthood (14.4% in *ubc-9(tm2610)*, compared to 25.3% in wild-type, $P < 0.0001$). Progeny survival in the *mre-11(ok179)*/nT1 strain was also reduced compared to wild-type (18.9% reach adulthood compared to 25.3% in wild-type, $P = 0.0053$). The double *ubc-9(tm2610);mre-11(ok179)* mutant progeny have further reduced larval and adult survival compared to wild-type (14.3% larval survival *vs.* 24.3% for wild-type; 8.4% adult survival *vs.* 25.3% in wild-type, $P < 0.0001$ for both). In addition, the double mutant had reduced survival to adulthood compared to each single mutant (8.4% *vs.* 14.4% in *ubc-9* and 18.9% in *mre-11(ok179)*, $P = 0.02$ and $P < 0.0001$, respectively) (Figure 4 and Table S6 in File S3).

We observed developmental effects in the *ubc-9(tm2610)*; *mre-11(ok179)* double mutants that were not apparent in the single mutants. Double-mutant worms that develop into adults take longer to reach adulthood (5–6 days after egg lay compared to 4 days in either single mutant). We observed that 100% of the double mutants that survived to adulthood were uncoordinated in their movement; this compares with 0% of *ubc-9(tm2610)* and *mre-11(ok179)* single mutants.

The *ubc-9(tm2610)*; *mre-11(ok179)* double-mutant gonads did not develop to normal wild-type volume and contained nuclei with abnormal DNA morphology (Figure 4A). Diakinesis was completely absent in this germline or there were up to two misshapen oocytes after late pachytene. We were not able to dissect *ubc-9*; *mre-11(ok179)* gonads due to their small size, precluding staining for RAD-51. To test if the double-mutant nuclei were still capable of entering meiosis, the assembly of the SC was used as a marker. We created a *syp-3*::*gfp*; *ubc-9(tm2610)*; *mre-11(ok179)* strain to visualize synapsis in whole worms without dissection. Despite abnormal DNA morphology, SYP-3 localized to chromosomes in a linear manner in "pachytene-like" nuclei (Figure 4A). This indicates that the double-mutant germline contains meiotic nuclei. Taken together, these data indicate that progression through meiosis in *ubc-9(tm2610)*; *mre-11(ok179)* gonads is severely affected, although meiotic entry does occur.

rad-50 or mre-11(iow1) mutations do not lead to synthetic sickness with ubc-9

In meiotic recombination, MRX/N has multiple roles, including structural roles such as tethering broken DNA and catalytic roles (*i.e.*, making DSBs and processing them to remove SPO-11 and create ssDNA) (Johzuka and Ogawa 1995; Nairz and Klein 1997; Moreau *et al.* 1999; Paull and Gellert 1999; van der Linden *et al.* 2009; Deshpande *et al.* 2014, 2016; Rojowska *et al.* 2014). One possibility for the deleterious phenotype observed in the germline in *ubc-9(tm2610)*; *mre-11(ok179)* double mutants is due to the complete loss of all MRE-11 roles. Alternatively, it could be due to a specific MRE-11 function. To test the role of meiotic DSB formation in the synthetic sick germline phenotype, we created a double mutant in which only the resection activity of MRE-11 is compromised in the *ubc-9* null background. *ubc-9(tm2610)*; *mre-11(iow1)* double mutants formed germlines comparable in size to *ubc-9(tm2610)* and exhibited a RAD-51 localization pattern similar to that observed in the *ubc-9(tm2610);spo-11(ok79)* strain (Figure 2 and Figure S4 in File S1). This data indicates that the synthetic lethal interaction between *ubc-9* and *mre-11* is dependent on MRE-11's function outside of its catalytic activity.

To determine if the synthetic sick interaction was specific to *ubc-9* and *mre-11*, or if any member of the MRX/N complex would produce the same result, we created a *ubc-9(tm2610)*; *rad-50(ok97)* double mutant and assessed gonad morphology and larval lethality in this mutant as was done in Figure 4B. *rad-50(ok97)* is a null mutation. There was no difference in hatch or growth rate in *ubc-9*; *rad-50* double mutants compared to *ubc-9* mutants (Figure 4B and Figure S6 in File S2). Germline morphology of the *ubc-9*; *rad-50* double mutants was indistinguishable from that of *ubc-9* single mutants (Figure 4 and data not shown). These data indicate that the sickness found in *ubc-9(tm2610)*; *mre-11(ok179)* double mutants is specifically due to the absence of MRE-11 rather than the complete MRX/N complex (see *Discussion*).

UBC-9 localization is MRE-11-independent

The MRX/N complex is known to localize to DNA since it acts directly at sites of DNA damage (Desai-Mehta *et al.* 2001; Robison *et al.* 2004). If MRE-11 and UBC-9 interact *in vivo*, the nuclear localization of one may be dependent on the other. We created a *mre-11*::*gfp* strain through CRISPR/Cas9 genome editing to visualize MRE-11 localization in a *ubc-9 (tm2610)* mutant background. *mre-11*::*gfp* worms are a viable and fertile strain, indicating that insertion of *gfp* likely does not perturb any function of MRE-11. In wild-type strains, MRE-11::GFP localizes to meiotic nuclei in all stages of meiosis through the end of pachytene (Figure S7 in File S2), similarly to what is found in immunolocalization studies (Goodyer *et al.* 2008). We did not see a difference in the MRE-11 localization pattern between wild-type and *ubc-9(tm2610)* strains (Figure S7 in File S2). We then tested whether FLAG::UBC-9 localization was affected in *mre-11(ok179)* mutants. FLAG::UBC-9 was still able to localize in pachytene nuclei in the absence of *mre-11* (Figure S8 in File S2). The intensity of FLAG::UBC-9 in PMT nuclei was measured and no significant change was detected. We conclude that UBC-9 and MRE-11 localize to meiotic nuclei independently of each other.

Mitotic proliferation is decreased in SUMOylation mutants

The increase in RAD-51 foci in the PMT in SUMOylation mutants suggests that the repair of DNA damage generated during replication (such as collapsed replication forks) is

A

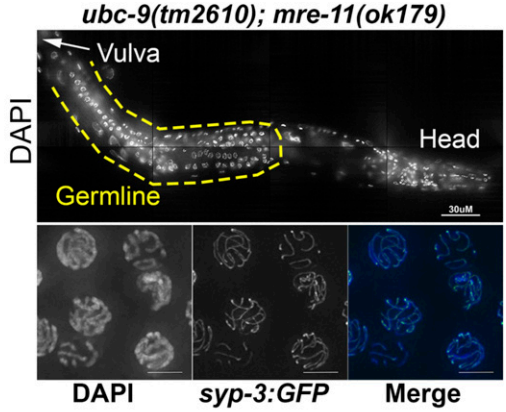

B

P0 Genotype	% eggs hatched	% larvae becoming adults	% GFP negative larvae	% GFP negative adults	Number of replicates
+/nT1	100 ± 1.6	100 ± 0.6	24.3 ± 1.8	25.3 ± 0.6	3
ubc-9(tm2610)/nT1	45.5 ± 2.2	81.7 ± 2.2	17.1 ± 1.4	13.3 ± 1.5	7
mre-11(ok179)/nT1	41.8 ± 2.0	92.5 ± 5.3	16.9 ± 1.7	18.9 ± 1.6	7
ubc-9(tm2610); mre-11(ok179)/nT1	40.1 ± 4.9	88.7 ± 7.1	14.3 ± 2.8	8.4 ± 2.2	7
rad-50(ok97)/nT1	43.0 ± 0.8	97.3 ± 3.2	24.1 ± 2.2	24.3 ± 2.2	3
ubc-9(tm2610);rad-50(ok97)/nT1	38.6 ± 5.5	81 ± 7.4	19.5 ± 4.2	16.6 ± 4.1	3

Figure 4 *ubc-9(tm2610); mre-11(ok179)* double mutants have underdeveloped germlines and have slowed larval development and survival. (A) DAPI-stained half worm of *ubc-9(tm2610); mre-11 (ok179)* double mutant. The middle of the worm is oriented to the left (arrow labeled "vulva" points to its location). The germline is outlined in a yellow dashed line. *syp-3*::*gfp* was crossed into the double-mutant background and whole worms were fixed. SYP-3::GFP linearization was observed in nuclei toward the end of the germline indicating that pairing occurs in these mutants. (B) Larval lethality of broods laid from balanced hermaphrodites of various genotypes. All genotypes are balanced over nT1(gfp). Between three and seven replicates of each genotype were counted. Pairwise comparisons (Fisher's exact *t*-test) are in the supplement. Percentages of $GFP^{+/-}$ larvae and $GFP^{+/-}$ adults were calculated to determine if there is increased lethality among the GFP^{-} (homozygous) offspring. Mean ± SEM is given for all percentages.

SUMOylation-dependent. DNA damage can trigger cell cycle arrest leading to reduced mitotic proliferation, which could explain the reduction in germline size (Gartner *et al.* 2000). To test this hypothesis, we examined the percentage of M- and S-phase nuclei in the PMT in our mutants.

To determine how S-phase is affected in SUMOylation mutants, we stained dissected gonads with an antibody to PCN-1, *C. elegans* PCNA (Kim and Michael 2008). PCNA is essential for replication and a good marker for S-phase nuclei (Celis *et al.* 1987; Prelich *et al.* 1987). We calculated the percentage of PCN-1-positive cells in the PMT in all genetic backgrounds examined in this paper (Figure 5A and Table S8 in File S3). Both the *mre-11(ok179)* strain and the *ubc-9;mre-11(iow1)* double-mutant strain had fewer S-phase nuclei compared to the wild-type strain (36.8 and 36.9% compared to 50.5%; $P < 0.0001$ for both comparisons, $n = 5$ PMTs/genotype). No difference in the percentage of S-phase nuclei was found for the other genotypes (Figure 5A and Table S8 in File S3).

PH3 in worms marks metaphase nuclei (Hendzel *et al.* 1997). The percentage of PH3-positive nuclei is defined as the MI (MI = $PH3^{+}$ PMT nuclei/total PMT nuclei × 100), which correlates with the percentage of mitotically dividing germline nuclei (Crittenden and Kimble 2008). Wild-type worms had an MI of 4%, which was significantly higher than that of both SUMOylation mutants (Figure 5B and Table S9 in File S3; 1.66%, $P = 0.0003$ for *ubc-9(tm2610)*, and 0.57%, $P < 0.0001$ for *smo-1(ok359)* mutants). The total number of nuclei present in the PMT of SUMOylation mutants was also reduced compared to wild-type (average: wild-type 205.8, *ubc-9(tm2610)* 144.5, and *smo-1(ok359)* 121).

mre-11 and ubc-9 mutants are delayed in RAD-51 loading in response to replication stress

SUMOlyation mutants had reduced PMT nuclei in S-phase and an increased number of RAD-51 foci. Both of these results are consistent with the presence of increased damage in the PMT. We introduced replication stress in wild-type, *ubc-9(tm2610)*, and *mre-11(ok179)* mutants by using the chemicals HU and CPT. HU depletes dNTP pools and causes polymerase to stall, while CPT inhibits topoisomerase I (TOP-1) (Fox 1985; Porter and Champoux 1989; Gedik and Collins 1990) (Figure 6). These chemicals test the reaction of *ubc-9* and *mre-11* null mutants to replication stresses (Kim and Colaiacovo 2014, 2015). Since neither *ubc-9* nor *mre-11* null mutants produce viable offspring, it is not possible to test the effects of these chemicals on progeny numbers. Instead, we analyzed the effect of HU and CTP on RAD-51 foci in the gonad following an 8-hr exposure. As expected, wild-type worms had increased RAD-51 foci in response to both drugs compared to controls. The *mre-11(ok179)* mutant exposed to HU did not show a significant increase in PMT RAD-51 foci compared to wild-type nuclei and only began to increase in RAD-51 foci at the 6-hr time-point (Figure 6A). CPT response was comparable to wild-type in the *mre-11(ok179)* background (Figure 6B). *ubc-9(tm2610)* mutants exposed to HU showed minimal increase over 8 hr, while exposure to CTP led to a smaller increase compared to nonexposed nuclei, but still significantly less than wild-type at 8 hr (Figure 6). This data indicates that both MRE-11 and UBC-9 are required for the formation of the ssDNA-RAD-51 filament following replication stress at the time intervals examined.

Interfering crossovers are not affected in ubc-9 mutants, however noninterfering crossover pathways may be increased

C. elegans is an organism in which crossover interference is complete; HR ultimately results in a single interfering crossover per chromosome pair, for a total of six crossovers per nucleus (Goldstein and Slaton 1982). DAPI bodies observed in *ubc-9* mutants look aberrant, with elongated, multiple

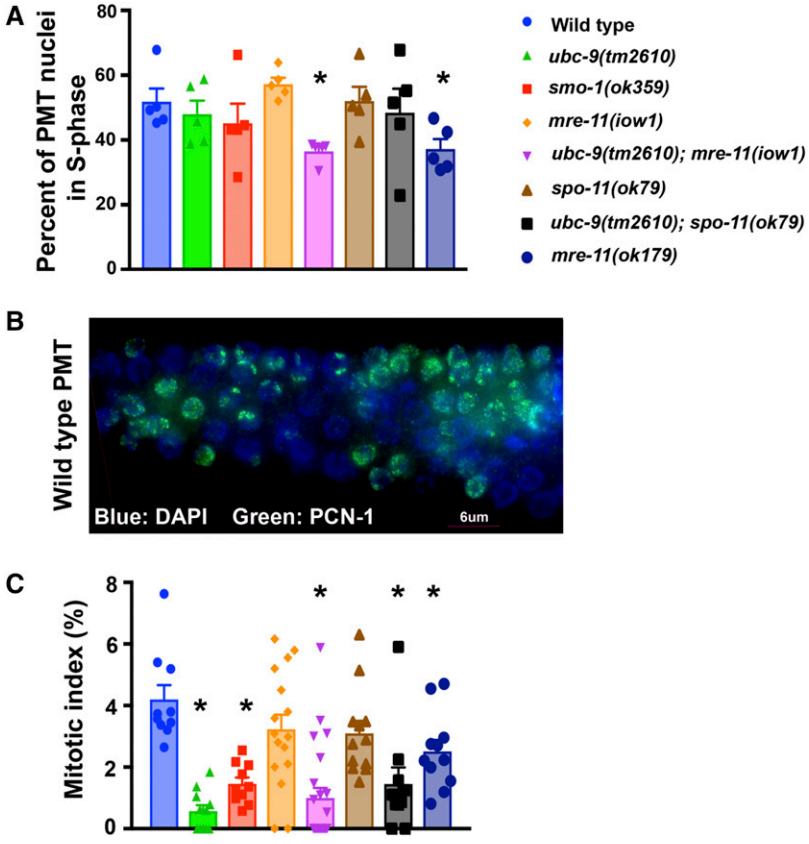

Figure 5 SUMOylation mutants have wild-type levels of PCN-1-positive nuclei but exhibit a decrease in M-phase nuclei. (A) Germlines of various genotypes were stained with an antibody to PCN-1 and the number of PCN-1$^+$ nuclei counted; the number was divided by the total number of nuclei in the premeiotic tip (PMT). Five PMTs of each genotype were counted. (B) Example of PCN-1 staining in a wild-type PMT. The distal tip of the gonad is oriented to the left. PCN-1 is green, DAPI is blue. (C) Germlines were stained for phospho-histone 3 (PH3). The mitotic index was calculated as PH3$^+$ PMT nuclei/total PMT nuclei. At least 10 PMTs were counted per genotype. Error bars signify the mean ± SEM. Pairwise comparisons can be found in the supplement (Fisher's exact test).

pinched regions along the chromosomes instead of the cruciform structure observed in wild-type (Figure 7, A and B). The abnormal *ubc-9* morphology could be explained if there were more than one crossover per bivalent in SUMOylation mutants.

To test this hypothesis, we first tested if the pinched regions are a visual manifestation of crossovers in our mutants. Based on RAD-51 foci counts, it is likely that in *ubc-9*; *spo-11* double mutants, DSBs are reduced but not eliminated (since DSBs are carried over from mitosis to meiosis). These mutants still maintain the aberrant chromosomal morphology of *ubc-9(tm2610)* mutants but are expected to have less crossovers. If pinched regions are synonymous to crossovers, then their frequency should decrease in *ubc-9*; *spo-11* double mutants compared to *ubc-9(tm2610)* mutants. Indeed, DAPI body counts in *ubc-9*; *spo-11* double mutants are intermediate between that found in each single mutant, indicating that crossovers are present but reduced in the double mutants (Figure 7C, left top). Accordingly, the number of pinched regions is reduced as well (Figure 7C, right top). There is a correlation between bivalent length and the number of pinched regions; bigger DAPI bodies that are more likely to be bivalents are more likely to have increased numbers of pinched regions (Figure 7C, bottom and Figure S10 in File S2).

To test if crossovers are increased in *ubc-9(tm2610)* mutants, we created a *cosa-1*::*gfp*; *ubc-9(tm2610)* strain. COSA-1 marks interfering crossover sites in *C. elegans* (Yokoo *et al.* 2012). Six COSA-1 foci are observed per nucleus in a wild-type background; six COSA-1 foci are also observed per nucleus in *ubc-9(tm2610)* mutants (Figure S9 in File S2 and Table S10 in File S3). Elevated levels of recombination could still occur, either as noninterfering crossovers or as events resolved as noncrossovers.

We next measured recombination frequency to assess both interfering and noninterfering crossovers. In wild-type *C. elegans*, all crossovers are interfering, but some mutants show increases in noninterfering crossovers without affecting interfering crossovers (Youds *et al.* 2010). It is not possible to measure recombination frequencies in null SUMOylation mutants because they are sterile. Therefore, we examined a heterozygous *ubc-9(tm2610)/+* strain in the hope that it might be haploinsufficient. A heterozygous *ubc-9(tm2610)/+* strain was generated from a cross between balanced heterozygotes, *ubc-9(tm2610)/nT1* in the Bristol background and wild-type males from the Hawaiian *C. elegans* background. Recombination frequencies were compared to wild-type hermaphrodites generated by a cross between N2 (Bristol) and Hawaiian strains (Table S11 in File S3). We performed SNP analysis for two loci on chromosome II that have been published to be 29 map units (m.u.) apart (Wicks *et al.* 2001; Swan *et al.* 2002). F2 progeny were scored for recombination events. The wild-type worms had a recombination frequency of 33 m.u, which is not significantly different from the expected recombination frequency of 29 m.u. However, the *ubc-9(tm2610)* heterozygotes had a recombination frequency of 50.3 m.u., which is significantly higher than the wild-type background cross ($P = 0.0016$) and

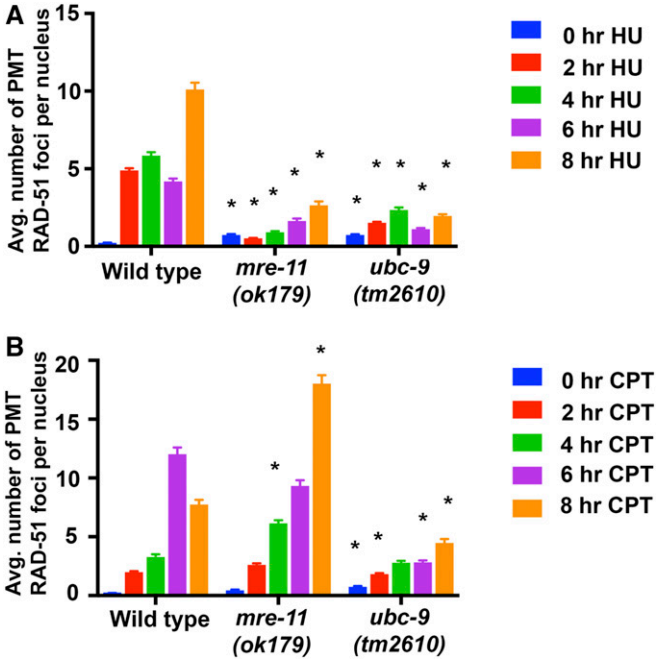

Figure 6 *ubc-9(tm2610)* and *mre-11(ok179)* mutants show defects in average (Avg.) RAD-51 recruitment following HU (hydroxyurea) and CPT (camptothecin) exposure in premeiotic tip (PMT) nuclei. (A) Graph of RAD-51 foci counts after 5.25 mM HU exposure over an 8-hr period. Controls were not exposed to any chemical. At least three PMTs were counted per genotype (826–1626 total PMT nuclei counted per treatment). Stars indicate $P < 0.05$ compared to wild-type at the equivalent time-point (Mann–Whitney *U* test). Other pairwise comparisons can be found in supplemental tables. (B) Graph of RAD-51 foci counts after 350 nM CPT exposure over an 8-hr period. Three to eight PMTs were counted in each of the time-points and for each genotype (668–1719 total PMT nuclei counted per treatment). Error bars signify the mean ± SEM. Stars indicate $P < 0.05$ compared to wild-type at the equivalent time-point (Mann–Whitney *U* test).

the published recombination frequency (p). Additional analysis was performed for chromosome I across a smaller genomic interval. Expected recombination frequency was 11 m.u., wild-type was 20.4 m.u., and *ubc-9* heterozygotes had a recombination frequency of 37.8 m.u. The difference between the wild-type and the *ubc-9* heterozygotes was significant ($P = 0.014$). These data are consistent with the view that recombination frequency is increased in *ubc-9* heterozygotes. These data support the hypothesis that even though interfering crossovers are not affected by SUMOylation loss, total crossovers appear to be increased, suggesting that SUMOylation normally plays a role in downregulating crossover numbers in *C. elegans*.

EMO nuclei are found in SUMOylation mutants

Diakinesis contains an average of 8.5 ± 0.27 nuclei in wild-type germlines. *ubc-9(tm2610)* mutants have an average of 5.4 ± 0.34 total diakinesis nuclei and *smo-1(ok359)* mutants have an average of 3.9 ± 0.36 total diakinesis nuclei. Mutant *ubc-9* diakinesis nuclei also contained endomitotic nuclei (Cremona *et al.* 2012) (Figure 7). These are diakinesis oocytes that prematurely replicate their DNA prior to the end of meiosis I leading to a decondensed mass of DNA, and present as a bright ball of DNA stained with DAPI (Iwasaki *et al.* 1996). EMO nuclei were found in both single SUMOylation mutants, while they were never found in wild-type worms of the same age (Figure 7 and Table S12 in File S3). *ubc-9(tm2610)* mutants had at least one EMO nucleus in diakinesis, with an average of 40% of total nuclei in diakinesis being EMO. This phenotype was not as prevalent in *smo-1(ok359)* mutants, with only 10% of total diakinesis nuclei being EMO. All *ubc-9(tm2610)* EMO nuclei stained brightly for replication protein PCN-1 compared to the haze of PCN-1 not localized to chromatin in wild-type diakinesis nuclei (Figure 7C).

We wondered whether the EMO phenotype observed in SUMOlyation mutants might be caused by the increased level of recombination that we had observed (see above). To test this, we analyzed the double-mutant strains *ubc-9(tm2610) mre-11(iow1)* and *ubc-9(tm2610) spo-11* for EMO nuclei in diakinesis. The *spo11* mutation prevents all meiotic recombination, and the *mre-11(iow1)* mutation blocks recombination after DSB formation. EMO formation was not detectably altered compared to the single *ubc-9* mutant background. These data indicate that SUMOylation is important to prevent premature replication independently of its role in controlling recombination and preventing DNA damage repair (Figure 8).

Discussion

The SUMO protein is a modification present in all eukaryotes that is highly conserved at the amino acid level. SUMO has a wider range of functions than its structural cousin, ubiquitin. Despite the important role SUMOylation plays in development, it is not essential for viability (M^+Z^-) in *C. elegans*. In this paper, we discovered a number of roles for SUMOylation in the *C. elegans* germline; SUMOylation is important for nuclear proliferation by preventing the accumulation of unrepaired DNA damage, affects the number of crossovers, and prevents replication in late meiotic prophase I nuclei. We also described a genetic interaction between *ubc-9* and *mre-11* in *C. elegans* that was previously unknown.

SUMOylation pathway proteins localize to germline nuclei and genetically interact with mre-11

SUMO and UBC-9 proteins are enriched in the nucleus and UBC-9 is present at the nuclear periphery in wild-type germlines [our study and Pelisch *et al.* (2017)]. Analysis of the *ubc-9* mutation combined with the *mre-11* null mutation implies that the double mutant displays a synergistic effect. The phenotypes conferred by the *mre-11(iow1)* and *mre-11(ok179)* alleles, when coupled with the *ubc-9(tm2610)* allele, suggest that resection activity is not responsible for the different phenotypes. Neither allele has resection activity. One explanation could be a structural role for MRE-11. This hypothesis is consistent with MRE-11 interacting with multiple proteins that are key players in various aspects of DSB repair (Williams *et al.* 2007, 2009). The *ubc-9(tm2610);mre-11(ok179)* synergistic

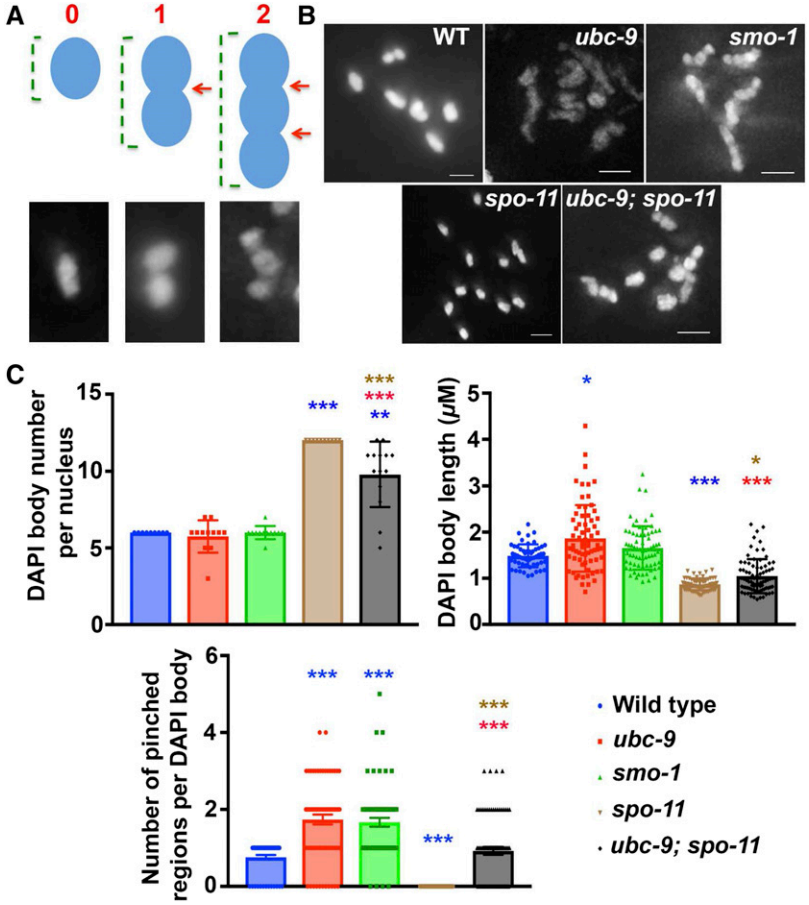

Figure 7 *spo-11* mutant univalent phenotype is partially rescued in *ubc-9;spo-11* double-mutant diakinesis. (A) Schematic of how DAPI bodies were measured in this figure. Univalents do not have any pinched regions, normal bivalents (middle) have one pinched region (red arrow), and an example of an aberrant DAPI body with more than one pinched region is displayed on the right. Green brackets indicate how the length measurement was obtained in (C). (B) Representative images of diakinesis nuclei from all genotypes measured. Bar, 1.5 μM. (C) Graphs of all five genotypes measuring the number of DAPI bodies per nucleus, length of each DAPI body within a nucleus, and the number of pinched regions per DAPI body within a nucleus. Between 10 and 14 nuclei were analyzed, and for individual DAPI body measurements 54–79 DAPI bodies were measured per genotype. Mann–Whitney *U* test was performed on all pairwise groups and the stars above data indicate significance. The color corresponds to the genotype with which the data is significantly different [*i.e.*, blue stars are being compared with wild-type (WT)]. *** $P < 0.0001$, ** $P < 0.001$, and * $P < 0.05$.

interaction would be consistent with the MRE-11 and UBC-9 proteins affecting the same biological function, albeit with distinct mechanisms.

SUMOylation is required both for preventing DNA damage and for the proliferation of mitotically cycling cells in the hermaphrodite germline

Mice with mutations in SUMO1, SUMO2, or UBC9 arrest in early embryonic development and do not survive past birth (Nacerddine *et al.* 2005). Developmental defects are also seen in zebrafish where SUMOylation defects are associated with increased apoptosis, polyploidization, and defects in the G2/M-phase of the cell cycle; there is no effect on S-phase (Nowak and Hammerschmidt 2006). Staining for the PCNA homolog (PCN-1) in the PMT of the *C. elegans* germline showed no significant difference between SUMOylation mutants and a wild-type strain in the fraction of nuclei in S-phase, but we did observe that the M-phase fraction of nuclei was reduced in SUMOylation mutants. A reduction in M-phase nuclei could stem from reduced M-entry or accelerated M-exit. Because SUMOylation mutant germlines contain fewer overall nuclei, we favor the former explanation.

One explanation for the PMT defects observed in SUMOylation mutants is the activation of a G2 (G2/M) checkpoint that recognizes defects occurring in S-phase. The *smo-1(ok359)* and *ubc-9(tm2610)* mutants both show increased numbers of RAD-51 foci in the PMT indicating increased DNA damage. Since PMT cells are cycling (~50% are in S-phase, Figure 5), we posit that the damage is caused by replication fork stalling and collapse (Cha and Kleckner 2002). Many replication and repair proteins (including RPA, PCNA, BLM, and TopII) are known to be SUMOylated in other organisms upon replication stalling (Pfander *et al.* 2005; Takahashi *et al.* 2008; Gali *et al.* 2012; Ouyang *et al.* 2013; Wu and Zou 2016). If this type of SUMOylation occurs in worms, the increase in DNA damage in the PMT may result from aberrant function of one or more of these proteins. So far, we have excluded RAD-51 as a SUMOylation target, while PCNA/PCN-1 was excluded by another group (Kim and Michael 2008). It is likely that ZTF-8, which acts in the 9-1-1 complex, is a target of SUMOylation (Kim and Colaiacovo 2015). However, the impairment of meiotic functions in *ztf-8* mutants (in the absence of DNA damage) is less severe compared to what is found in *ubc-9* mutants, indicating that ZTF-8 is not the only germline mitotic target of UBC-9 (Kim and Colaiacovo 2015). The complete array of S-phase SUMOylation targets in the *C. elegans* PMT awaits discovery.

Despite the presence of DNA damage in S-phase cells in SUMO mutants, the fraction of nuclei in S-phase is not affected by SUMOylation mutations. This implies that neither entry into, nor progression through, S-phase is affected by SUMOylation mutations; it further suggests that the mutations do not cause

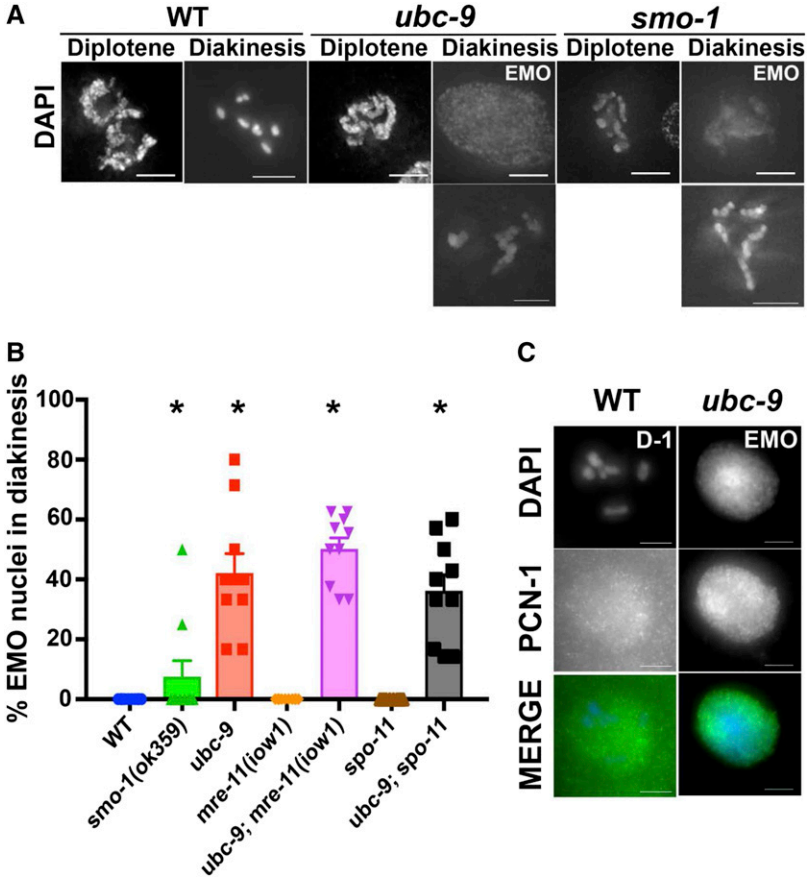

Figure 8 SUMOylation mutants have aberrant chromosomal morphology and EMO nuclei at diakinesis. (A) Representative images of diplotene and diakinesis nuclei in wild-type (WT), *ubc-9(tm2610)*, and *smo-1(ok359)* strains. Both EMO and non-EMO phenotypes are shown for mutants. Mutant non-EMO oocytes still had abnormal morphology compared to WT. Points on the graph indicate individual data points, with the bar indicating the mean of all data points. (B) Percentage of EMO nuclei counted from DAPI-stained whole worms. At least 10 worms from each genotype were counted. Error bars signify the mean ± SEM. (C) Representative EMO oocyte from a *ubc-9(tm2610)* gonad staining strongly for PCN-1. WT oocytes have low levels of background PCN-1 staining not associated with chromatin. Ten WT D-1 oocytes and 11 EMO oocytes were counted for PCN-1 staining. Points on the graph indicate individual data points, with the bar indicating the mean of all data points.

activation of an S-phase checkpoint. In mammalian cells, the E3 SUMO ligase PIAS3 is required to SUMOylate ATR so that it can be activated through autophosphorylation in response to DNA damage to establish the S-phase checkpoint. (Wu and Zou 2016). Because ATR in *C. elegans* is also required for the S-phase checkpoint, the mammalian mechanism may explain the worm S-phase result (Garcia-Muse and Boulton 2005). In worm SUMOylation mutants, S-phase checkpoints appeared disabled and permitted cell cycle progression in the presence of damage. Because M-phase nuclei are decreased, the *C. elegans* G2/M checkpoint appears to be functional, and therefore not dependent on SUMOylation to function. We have also shown that the response to HU, in terms of RAD-51 focus formation, was attenuated in *ubc-9* mutants. This is consistent with the view that SUMOylation is needed for effective recruitment of RAD-51 following HU exposure.

To conclude, we propose that UBC-9 is required for the recruitment of RAD-51 after excess damage, to prevent replication fork collapse at the mitotic proliferating zone/PMT. In its absence, unrepaired DNA damage in the PMT triggers cell cycle arrest (likely at the G2/M transition) and thus reduces germline proliferation, leading to decreases in germline size. Since RAD-51 loading is impaired after excess damage but not prevented, the increase in DNA damage due to unrepaired DSBs ultimately causes and increase in the overall levels of RAD-51 foci.

Does SUMOylation play different roles in different types of cell visions in C. elegans?

In the germline, SMO-1 shows diffused nuclear localization [Pelisch and Hay (2016) and this study] but moves to the midbivalent regions upon nuclear envelope breakdown (Pelisch and Hay 2016]. In mitosis, SMO-1 shows a similar pattern, moving from diffused nuclear localization to specific localization on metaphase chromosomes (Pelisch *et al.* 2014). AIR-2 and KLP-19 proteins, which are present in the midbivalent region, are likely targets for SUMOylation, which is consistent with the localization pattern of SMO-1 (Pelisch and Hay 2016). Due to the early roles SUMOylation plays in the germline, studies of the meiotic and mitotic divisions of the embryo were performed by RNAi knockdown of *ubc-9*. These studies established the importance of SUMOylation in the congression of chromosomes at the metaphase plate, and therefore identified the key roles that they play in meiosis (Pelisch and Hay 2016). SUMOylation also controls the mitotic divisions in the embryo, targeting AIR-2, as found for mitosis (Pelisch *et al.* 2014). These studies reveal the importance of SUMOylation outside the germline and explain the embryonic lethality caused by the *ubc-9::flag*, which is likely to compromise the embryonic but not the germline function of SUMOylation.

We observed a reduction in M-phase nuclei in germline mitotic nuclei of both *smo-1* and *ubc-9* mutants, which is consistent with the reduction in the number of germline

nuclei. This may indicate a conserved metaphase function of SUMOylation in the mitotic germline as found in other dividing cells. However, we did not observe SMO-1 localized specifically to metaphase PMT chromosomes, nor an obvious congression defect in mitotic germline nuclei of *smo-1* and *ubc-9* mutants (Pelisch *et al.* 2014; Pelisch and Hay 2016). Due to the evident increase in RAD-51 foci in both *smo-1* and *ubc-9* mutants, we suggest that the proliferation defects in these mutants are due to checkpoint activation that prohibits M-phase entry and not due to defects in congression.

RAD-51 focus formation is altered in SUMO mutants

RAD-51 foci are typically present as individually defined foci of symmetrical appearance. However, in the SUMO mutants, the fraction of such atypical RAD-51 foci increased. Aberrant foci have been observed in mammalian cells when Rad51 was overexpressed, as well as in maize mutants defective in chromosome pairing during meiosis (Franklin *et al.* 1999; Raderschall *et al.* 2002; Pawlowski *et al.* 2003). Most of the atypical RAD-51 foci in single SUMOylation mutants are found in the PMT and then decrease throughout meiosis. After irradiation, the increased number of RAD-51 foci limits scoring of most classes of atypical foci with the exception of strings. Because the number of RAD-51 strings does not increase after radiation, their appearance in the PMT appears to be due to specific lesions, perhaps collapsed replication forks, which happen more frequently in SUMOylation mutants.

We hypothesize that atypical and typical foci represent two states of the same molecular event: a collapsed replication fork. In these events, a typical focus will contain two regions of ssDNA loaded with RAD-51, likely on sister chromatids, held together in close proximity. These RAD-51 foci on two sister chromatids would not be held together properly in our SUMOylation mutants. Doublets and other atypical RAD-51 foci could therefore represent a defect in the tethering of broken DNA molecules initiating from the same event of a collapsed replication fork, eventually leading to the broken DNA dissociating from one another.

ubc-9(tm2610);mre-11(ok179) double-mutant synthetic sickness is due to a function of MRE-11 other than resection

Double mutants lacking both MRE-11 and UBC-9 were slow-growing and fewer worms reached adulthood; they also exhibited a smaller germline compared to each single mutant, presumably due to less proliferation in the PMT. These results together point to an additive effect of MRE-11 and the SUMOylation pathway in promoting proper nuclear division prior to prophase I. These defects were not found in *ubc-9(tm2610);mre-11(iow1)* or *ubc-9(tm2610);rad-50(ok97)* double mutants, indicating that the role of MRE-11 in PMT events is specific to functions or structures still present in the *mre-11(iow1)* point mutant. One possibility is that the key role of the MRE-11 protein is a structural role in recruiting other proteins essential for DSB repair after S-phase damage (Lee and Paull 2005; Zheng *et al.* 2009; Shim *et al.* 2010; Nimonkar *et al.* 2011). If this were true, the different phenotype conferred by a *rad-50* null mutation suggests that the structural role is specific to MRE-11, not the MRX/N complex.

mre-11(iow1) single mutants have a small increase in atypical RAD-51 foci numbers compared to wild-type, but a larger effect is observed in *mre-11(ok179)* gonads. There is evidence in humans that MRE11 and the MRN/X complex are needed not only for resection during HR, but also during replication for tethering DNA, similar to the cohesin complex (de Jager *et al.* 2001; Seeber *et al.* 2016). In the PMT, the resection activity of MRE-11 is not absolutely essential due to the activity of other nucleases (Hayashi *et al.* 2007; Yin and Smolikove 2013) but, if MRE-11 protein is absent, the complex could not tether DNA molecules initiating from the same collapsed replication fork event, allowing the DNA ends to drift away from each other. The synthetic sickness of the *ubc-9*; *mre-11(ok179)* double mutants prevented us from analyzing RAD-51 localization in the PMT.

SUMOylation in yeast and mammalian cells is known to be involved in MRN/X complex function through either direct SUMOylation of the MRN/X complex proteins or through noncovalent SUMO interactions via Mre11's SIM domain in yeast (Chen *et al.* 2016). If this is true in *C. elegans*, this may explain why we uncovered UBC-9 and MRE-11 as physically interacting proteins by the yeast two-hybrid assay. It is possible that the absence of SUMOylation may destabilize the MRX/N complex in *C. elegans*, leading to atypical RAD-51 foci and increased lethality, but other SUMOylation functions would be MRE-11-independent. The latter could explain the synthetic sickness of the *ubc-9(tm2610)*;*mre-11(ok179)* double mutants. If so, MRE-11 noncovalent SUMO interaction would only be responsible for MRE-11's mitotic functions. This will explain why *ubc-9* and *mre-11* null mutants share phenotypes in PMT nuclei and not in prophase I.

The fraction of S-phase nuclei in the PMT were significantly decreased in *mre-11(ok179)* mutants; this could be due to MRE-11's role in replication initiation and/or to intra-S checkpoint activation (Olson *et al.* 2007). The delay in the loading of RAD-51 protein in *mre-11* mutants subjected to DNA damage agents is consistent with its role in resection to form ssDNA.

SUMOylation may play a role in meiotic recombination

We have shown that SUMOylation plays a role in germline proliferation in the PMT; this explains why SUMO mutants have reduced germline size. However, SUMOylation clearly has a role in later meiotic events. Our studies suggest that these meiotic roles are reserved for late events in DSB repair. Analysis of RAD-51 foci numbers indicates that the increase in meiotic foci in SUMOylation mutants compared to wild-type is primarily due to the effect of these mutations on PMT nuclei rather than a direct effect on meiosis. SUMOylation may also affect later meiotic events, such as crossover regulation. The number of interfering crossovers (measured by COSA-1 foci) is unchanged in the *ubc-9(tm2610)* mutant, but noninterfering crossovers are increased. One interpretation is

that some recombination events that normally would be resolved as noncrossovers are altered (Barber *et al.* 2008; Getz *et al.* 2008; Youds *et al.* 2010). The proposed increase in total crossovers is consistent with the appearance of diakinesis chromosomes that appear to have multiple chiasmata. These observations suggest that SUMOylation is involved in the mechanism regulating the outcome of recombination events. SUMOylation in mouse meiosis promotes crossovers at the expense of noncrossovers, likely by stabilizing the MSH-4/5 complex (Qiao *et al.* 2014; Rao *et al.* 2017). In *C. elegans*, the antirecombinase RTEL-1, along with DCC complex components, has been suggested to control the levels of noninterfering crossovers (Barber *et al.* 2008; Youds *et al.* 2010; Pferdehirt and Meyer 2013). It would be interesting if they were SUMOylation targets.

Some diakinesis nuclei in SUMOylation mutants appear to be undergoing replication based on PCNA localizing to the DNA. This observation suggests that SUMOylation could be required for repressing replication in the later stages of prophase I. There is no specific evidence that replication in late prophase I occurs in SUMOylation pathway mutants in other organisms, but in *Xenopus* the SUMO2/3 target is cyclin E, an early S-phase activator (Bonne-Andrea *et al.* 2013). When SUMO2/3 is depleted, increased origin firing occurs in the *Xenopus* cell-free system. The EMO phenotype that is observed in some diakinesis nuclei in SUMOylation mutants in late prophase I must contribute to their sterility. Since UBC-9 and SUMO were not detectable in diakinesis oocytes, their function in repressing rereplication must be established at earlier stages.

Conserved and divergent roles of SUMOylation in meiosis

C. elegans UBC-9 and SMO-1 are visible as peripheral or diffuse nuclear stains, respectively. These patterns differ from both yeast Ubc9 and mammalian Smct3 that localize to the SC (Kovalenko *et al.* 1996; Klug *et al.* 2013). SUMO chains that form along the SC in yeast stabilize the SC, promoting its proper assembly. The yeast SC protein Zip1 interacts directly with the SUMO-conjugated domain of SC protein Zip3 (Cheng *et al.* 2006). Unlike the role for SUMOylation in SC assembly in yeast, we and others (Bhalla *et al.* 2008) have not observed any defects in SC formation in SUMOylation mutants in *C. elegans*. In *C. elegans*, ZHP-3 was implicated in SUMO-mediated disassembly of the SC (Bhalla *et al.* 2008); although this may be a direct effect, aberrant SC localization in diakinesis can also stem from defects in bivalent restructuring in *ubc-9* mutants.

Study of the meiotic roles of the SUMOylation is difficult in vertebrates because null mutants are unable to complete embryonic development even when maternally loaded proteins are present in the early embryo (Mukai *et al.* 2006). In mammalian meiosis, the SUMO ligase RNF212 is required for proper Msh4/5 localization and crossover designation during HR (Reynolds *et al.* 2013). RNF212 is essential for crossover formation and SUMO is hypothesized to selectively stabilize crossover proteins at sites of recombination. We have also proposed that SUMOylation regulates crossover formation in *C. elegans*; however, this role is different: SUMOylation suppresses noninterfering crossovers in *C. elegans*, as opposed to promoting interfering crossovers as found in mouse.

Do SMO-1 and UBC-9 have similar but not identical functions?

smo-1 and *ubc-9* encode for the only SUMO and E2 in the SUMOylation pathway of *C. elegans*. Thus, *ubc-9(tm2610)* and *smo-1(ok359)* mutants are expected to exhibit the same phenotypes. Our analysis indicates that these two mutants indeed show very similar phenotypes. However, these phenotypes are not identical in their severity and most of the time *ubc-9(tm2610)* exhibits the more extreme phenotype. The *smo-1(ok359)* allele is a deletion of the whole reading frame of the gene, while the *ubc-9(tm2610)* allele removes just the sequences that encode for the catalytic domain of UBC-9. Therefore, the difference in the severity of the phenotypes cannot be explained by *smo-1(ok359)* mutants retaining SUMO activity. In other organisms, Ubc9 has catalysis-independent function (Chakrabarti *et al.* 1999; Poukka *et al.* 1999; Kurtzman and Schechter 2001). Therefore, loss-of-function mutations in the two genes may not lead to identical phenotypes. However, the fact that the overall phenotypes are very similar between the *ubc-9(tm2610)* and *smo-1 (ok359)* mutants indicates that if there is a catalysis-independent function for Ubc9, it has a relatively minor role. It is also possible that the *ubc-9(tm2610)* allele is not a complete deletion and some gain-of-function of the residual truncated protein modifies the phenotypes caused by the removal of SUMOylation in the germline. Again, if this is so, the effects are relatively small. A third option is that SUMO/SMO-1 is not depleted as quickly as UBC-9 during development and some maternally contributed SUMO is still present in the germline that will explain the differences.

Conclusions

Our studies are consistent with a central role for SUMO in DNA metabolism in worms, consistent with its established roles in mitosis and meiosis in many organisms. From our observations, we hypothesize that the meiotic functions of SUMOylation may vary substantially among different organisms, and to fully understand the breadth of its involvement it will need to be examined in multiple biological systems.

Acknowledgments

Some strains and clones were kindly provided by the *Caenorhabditis* Genetics Center, which is funded by the National Institutes of Health (NIH) Office of Research Infrastructure Programs (P40 OD-010440), and the *C. elegans* Reverse Genetics Core Facility at the University of British Columbia, which is part of the International *C. elegans* Gene Knockout Consortium. We thank the National Bioresource Project for the Experimental Animal "Nematode *C. elegans*", Japan for

providing the *tm2610* allele. We thank M. Michael for the PCN-1 antibody and M. Wheat for generation of the *mre-11*::*gfp* strain. We thank the Radiation and Free Radical Research Core Facility in the Carver College of Medicine for the irradiation service. This work was funded by NIH grant number 1R01 GM-112657 (to S.S.).

Literature Cited

Altmannova, V., N. Eckert-Boulet, M. Arneric, P. Kolesar, R. Chaloupkova *et al.*, 2010 Rad52 SUMOylation affects the efficiency of the DNA repair. Nucleic Acids Res. 38: 4708–4721.

Barber, L. J., J. L. Youds, J. D. Ward, M. J. McIlwraith, N. J. O'Neil *et al.*, 2008 RTEL1 maintains genomic stability by suppressing homologous recombination. Cell 135: 261–271.

Bascom-Slack, C. A., L. O. Ross, and D. S. Dawson, 1997 Chiasmata, crossovers, and meiotic chromosome segregation. Adv. Genet. 35: 253–284.

Bazan, G. C., and K. J. Hillers, 2011 SNP-based mapping of crossover recombination in Caenorhabditis elegans. Methods Mol. Biol. 745: 207–222.

Bernier-Villamor, V., D. A. Sampson, M. J. Matunis, and C. D. Lima, 2002 Structural basis for E2-mediated SUMO conjugation revealed by a complex between ubiquitin-conjugating enzyme Ubc9 and RanGAP1. Cell 108: 345–356.

Bhalla, N., D. J. Wynne, V. Jantsch, and A. F. Dernburg, 2008 ZHP-3 acts at crossovers to couple meiotic recombination with synaptonemal complex disassembly and bivalent formation in C. elegans. PLoS Genet. 4: e1000235.

Bishop, D. K., 1994 RecA homologs Dmc1 and Rad51 interact to form multiple nuclear complexes prior to meiotic chromosome synapsis. Cell 79: 1081–1092.

Bishop, D. K., D. Park, L. Xu, and N. Kleckner, 1992 DMC1: a meiosis-specific yeast homolog of E. coli recA required for recombination, synaptonemal complex formation, and cell cycle progression. Cell 69: 439–456.

Bocker, T., A. Barusevicius, T. Snowden, D. Rasio, S. Guerrette *et al.*, 1999 hMSH5: a human MutS homologue that forms a novel heterodimer with hMSH4 and is expressed during spermatogenesis. Cancer Res. 59: 816–822.

Bologna, S., V. Altmannova, E. Valtorta, C. Koenig, P. Liberali *et al.*, 2015 Sumoylation regulates EXO1 stability and processing of DNA damage. Nat. Cell Biol. 14: 2439–2450.

Bonne-Andrea, C., M. Kahli, F. Mechali, J. M. Lemaitre, G. Bossis *et al.*, 2013 SUMO2/3 modification of cyclin E contributes to the control of replication origin firing. Nat. Commun. 4: 1850.

Borde, V., W. Lin, E. Novikov, J. H. Petrini, M. Lichten *et al.*, 2004 Association of Mre11p with double-strand break sites during yeast meiosis. Mol. Cell 13: 389–401.

Boulton, S. J., J. S. Martin, J. Polanowska, D. E. Hill, A. Gartner *et al.*, 2004 BRCA1/BARD1 orthologs required for DNA repair in Caenorhabditis elegans. Curr. Biol. 14: 33–39.

Brenner, S., 1974 The genetics of Caenorhabditis elegans. Genetics 77: 71–94.

Broday, L., I. Kolotuev, C. Didier, A. Bhoumik, B. P. Gupta *et al.*, 2004 The small ubiquitin-like modifier (SUMO) is required for gonadal and uterine-vulval morphogenesis in Caenorhabditis elegans. Genes Dev. 18: 2380–2391.

Bylebyl, G. R., I. Belichenko, and E. S. Johnson, 2003 The SUMO isopeptidase Ulp2 prevents accumulation of SUMO chains in yeast. J. Biol. Chem. 278: 44113–44120.

Cao, L., E. Alani, and N. Kleckner, 1990 A pathway for generation and processing of double-strand breaks during meiotic recombination in S. cerevisiae. Cell 61: 1089–1101.

Celis, J. E., P. Madsen, A. Celis, H. V. Nielsen, and B. Gesser, 1987 Cyclin (PCNA, auxiliary protein of DNA polymerase delta) is a central component of the pathway(s) leading to DNA replication and cell division. FEBS Lett. 220: 1–7.

Cha, R. S., and N. Kleckner, 2002 ATR homolog Mec1 promotes fork progression, thus averting breaks in replication slow zones. Science 297: 602–606.

Chakrabarti, S. R., R. Sood, S. Ganguly, S. Bohlander, Z. Shen *et al.*, 1999 Modulation of TEL transcription activity by interaction with the ubiquitin-conjugating enzyme UBC9. Proc. Natl. Acad. Sci. USA 96: 7467–7472.

Chen, A., H. Mannen, and S. S. Li, 1998 Characterization of mouse ubiquitin-like SMT3A and SMT3B cDNAs and gene/pseudogenes. Biochem. Mol. Biol. Int. 46: 1161–1174.

Chen, Y. J., Y. C. Chuang, C. N. Chuang, Y. H. Cheng, C. R. Chang *et al.*, 2016 S. cerevisiae Mre11 recruits conjugated SUMO moieties to facilitate the assembly and function of the Mre11-Rad50-Xrs2 complex. Nucleic Acids Res. 44: 2199–2213.

Cheng, C. H., Y. H. Lo, S. S. Liang, S. C. Ti, F. M. Lin *et al.*, 2006 SUMO modifications control assembly of synaptonemal complex and polycomplex in meiosis of Saccharomyces cerevisiae. Genes Dev. 20: 2067–2081.

Chin, G. M., and A. M. Villeneuve, 2001 C. elegans mre-11 is required for meiotic recombination and DNA repair but is dispensable for the meiotic G(2) DNA damage checkpoint. Genes Dev. 15: 522–534.

Choudhury, B. K., and S. S. Li, 1997 Identification and characterization of the SMT3 cDNA and gene from nematode Caenorhabditis elegans. Biochem. Biophys. Res. Commun. 234: 788–791.

Citro, S., and S. Chiocca, 2013 Sumo paralogs: redundancy and divergencies. Front. Biosci. (Schol. Ed.) 5: 544–553.

Colaiacovo, M. P., A. J. MacQueen, E. Martinez-Perez, K. McDonald, A. Adamo *et al.*, 2003 Synaptonemal complex assembly in C. elegans is dispensable for loading strand-exchange proteins but critical for proper completion of recombination. Dev. Cell 5: 463–474.

Cremona, C. A., P. Sarangi, Y. Yang, L. E. Hang, S. Rahman *et al.*, 2012 Extensive DNA damage-induced sumoylation contributes to replication and repair and acts in addition to the mec1 checkpoint. Mol. Cell 45: 422–432.

Crittenden, S. L., and J. Kimble, 2008 Analysis of the C. elegans germline stem cell region. Methods Mol. Biol. 450: 27–44.

de Jager, M., M. L. Dronkert, M. Modesti, C. E. Beerens, R. Kanaar *et al.*, 2001 DNA-binding and strand-annealing activities of human Mre11: implications for its roles in DNA double-strand break repair pathways. Nucleic Acids Res. 29: 1317–1325.

Dernburg, A. F., K. McDonald, G. Moulder, R. Barstead, M. Dresser *et al.*, 1998 Meiotic recombination in C. elegans initiates by a conserved mechanism and is dispensable for homologous chromosome synapsis. Cell 94: 387–398.

Desai-Mehta, A., K. M. Cerosaletti, and P. Concannon, 2001 Distinct functional domains of nibrin mediate Mre11 binding, focus formation, and nuclear localization. Mol. Cell. Biol. 21: 2184–2191.

Deshpande, R. A., G. J. Williams, O. Limbo, R. S. Williams, J. Kuhnlein *et al.*, 2014 ATP-driven Rad50 conformations regulate DNA tethering, end resection, and ATM checkpoint signaling. EMBO J. 33: 482–500.

Deshpande, R. A., G. J. Williams, O. Limbo, R. S. Williams, J. Kuhnlein *et al.*, 2016 ATP-driven Rad50 conformations regulate DNA tethering, end resection, and ATM checkpoint signaling. EMBO J. 35: 791.

Dickinson, D. J., and B. Goldstein, 2016 CRISPR-based methods for Caenorhabditis elegans genome engineering. Genetics 202: 885–901.

Dresser, M. E., D. J. Ewing, M. N. Conrad, A. M. Dominguez, R. Barstead *et al.*, 1997 DMC1 functions in a Saccharomyces

cerevisiae meiotic pathway that is largely independent of the RAD51 pathway. Genetics 147: 533–544.
Edgley, M. L., D. L. Baillie, D. L. Riddle, and A. M. Rose, 2006 Genetic balancers (April 6, 2006). WormBook, ed. The *C. elegans* Research Community, WormBook, doi/10.1895/wormbook.1.89.1, http://www.wormbook.org.
Falck, J., J. V. Forment, J. Coates, M. Mistrik, J. Lukas *et al.*, 2012 CDK targeting of NBS1 promotes DNA-end resection, replication restart and homologous recombination. EMBO Rep. 13: 561–568.
Ferreira, H. C., B. D. Towbin, T. Jegou, and S. M. Gasser, 2013 The shelterin protein POT-1 anchors Caenorhabditis elegans telomeres through SUN-1 at the nuclear periphery. J. Cell Biol. 203: 727–735.
Fox, R. M., 1985 Changes in deoxynucleoside triphosphate pools induced by inhibitors and modulators of ribonucleotide reductase. Pharmacol. Ther. 30: 31–42.
Franklin, A. E., J. McElver, I. Sunjevaric, R. Rothstein, B. Bowen *et al.*, 1999 Three-dimensional microscopy of the Rad51 recombination protein during meiotic prophase. Plant Cell 11: 809–824.
Galanty, Y., R. Belotserkovskaya, J. Coates, and S. P. Jackson, 2012 RNF4, a SUMO-targeted ubiquitin E3 ligase, promotes DNA double-strand break repair. Genes Dev. 26: 1179–1195.
Gali, H., S. Juhasz, M. Morocz, I. Hajdu, K. Fatyol *et al.*, 2012 Role of SUMO modification of human PCNA at stalled replication fork. Nucleic Acids Res. 40: 6049–6059.
Garcia-Muse, T., and S. J. Boulton, 2005 Distinct modes of ATR activation after replication stress and DNA double-strand breaks in Caenorhabditis elegans. EMBO J. 24: 4345–4355.
Gartner, A., S. Milstein, S. Ahmed, J. Hodgkin, and M. O. Hengartner, 2000 A conserved checkpoint pathway mediates DNA damage–induced apoptosis and cell cycle arrest in C. elegans. Mol. Cell 5: 435–443.
Gedik, C. M., and A. R. Collins, 1990 Comparison of effects of fostriecin, novobiocin, and camptothecin, inhibitors of DNA topoisomerases, on DNA replication and repair in human cells. Nucleic Acids Res. 18: 1007–1013.
Getz, T. J., S. A. Banse, L. S. Young, A. V. Banse, J. Swanson *et al.*, 2008 Reduced mismatch repair of heteroduplexes reveals "non"-interfering crossing over in wild-type Saccharomyces cerevisiae. Genetics 178: 1251–1269.
Goldstein, P., and D. E. Slaton, 1982 The synaptonemal complexes of Caenorhabditis elegans: comparison of wild-type and mutant strains and pachytene karyotype analysis of wild-type. Chromosoma 84: 585–597.
Goodyer, W., S. Kaitna, F. Couteau, J. D. Ward, S. J. Boulton *et al.*, 2008 HTP-3 links DSB formation with homolog pairing and crossing over during C. elegans meiosis. Dev. Cell 14: 263–274.
Greenwald, I., 1997 Development of the vulva in *C. elegans II*, edited by D. L. Riddle, T. Blumenthal, B. J. Meyer, and J. R. Priess. Cold Spring Harbor Laboratory Press, Cold Spring Harbor, NY.
Guzzo, C. M., C. E. Berndsen, J. Zhu, V. Gupta, A. Datta *et al.*, 2012 RNF4-dependent hybrid SUMO-ubiquitin chains are signals for RAP80 and thereby mediate the recruitment of BRCA1 to sites of DNA damage. Sci. Signal. 5: ra88.
Haas, A. L., J. V. Warms, A. Hershko, and I. A. Rose, 1982 Ubiquitin-activating enzyme. Mechanism and role in protein-ubiquitin conjugation. J. Biol. Chem. 257: 2543–2548.
Habu, T., T. Taki, A. West, Y. Nishimune, and T. Morita, 1996 The mouse and human homologs of DMC1, the yeast meiosis-specific homologous recombination gene, have a common unique form of exon-skipped transcript in meiosis. Nucleic Acids Res. 24: 470–477.
Hayashi, M., G. M. Chin, and A. M. Villeneuve, 2007 C. elegans germ cells switch between distinct modes of double-strand break repair during meiotic prophase progression. PLoS Genet. 3: e191.
Hendzel, M. J., Y. Wei, M. A. Mancini, A. Van Hooser, T. Ranalli *et al.*, 1997 Mitosis-specific phosphorylation of histone H3 initiates primarily within pericentromeric heterochromatin during G2 and spreads in an ordered fashion coincident with mitotic chromosome condensation. Chromosoma 106: 348–360.
Hohl, M., Y. Kwon, S. M. Galvan, X. Xue, C. Tous *et al.*, 2011 The Rad50 coiled-coil domain is indispensable for Mre11 complex functions. Nat. Struct. Mol. Biol. 18: 1124–1131.
Hollingsworth, N. M., L. Ponte, and C. Halsey, 1995 MSH5, a novel MutS homolog, facilitates meiotic reciprocal recombination between homologs in Saccharomyces cerevisiae but not mismatch repair. Genes Dev. 9: 1728–1739.
Holway, A. H., S. H. Kim, A. La Volpe, and W. M. Michael, 2006 Checkpoint silencing during the DNA damage response in Caenorhabditis elegans embryos. J. Cell Biol. 172: 999–1008.
Hooker, G. W., and G. S. Roeder, 2006 A role for SUMO in meiotic chromosome synapsis. Curr. Biol. 16: 1238–1243.
Horigome, C., D. E. Bustard, I. Marcomini, N. Delgoshaie, M. Tsai-Pflugfelder *et al.*, 2016 PolySUMOylation by Siz2 and Mms21 triggers relocation of DNA breaks to nuclear pores through the Slx5/Slx8 STUbL. Genes Dev. 30: 931–945.
Horvitz, H. R., and P. W. Sternberg, 1991 Multiple intercellular signalling systems control the development of the Caenorhabditis elegans vulva. Nature 351: 535–541.
Hu, Y., and J. D. Parvin, 2014 Small ubiquitin-like modifier (SUMO) isoforms and conjugation-independent function in DNA double-strand break repair pathways. J. Biol. Chem. 289: 21289–21295.
Huang, H. W., S. C. Tsoi, Y. H. Sun, and S. S. Li, 1998 Identification and characterization of the SMT3 cDNA and gene encoding ubiquitin-like protein from Drosophila melanogaster. Biochem. Mol. Biol. Int. 46: 775–785.
Hubbard, E. J. A., and G. David, 2005 Introduction to the germ line (September 1, 2005). *WormBook*, ed. The C. *elegans* Research Community, WormBook, doi/10.1895/wormbook.1.18.1, http://www.wormbook.org.
Ismail, I. H., J. P. Gagne, M. M. Genois, H. Strickfaden, D. McDonald *et al.*, 2015 The RNF138 E3 ligase displaces Ku to promote DNA end resection and regulate DNA repair pathway choice. Nat. Cell Biol. 17: 1446–1457.
Iwasaki, K., J. McCarter, R. Francis, and T. Schedl, 1996 emo-1, a Caenorhabditis elegans Sec61p gamma homologue, is required for oocyte development and ovulation. J. Cell Biol. 134: 699–714.
Johzuka, K., and H. Ogawa, 1995 Interaction of Mre11 and Rad50: two proteins required for DNA repair and meiosis-specific double-strand break formation in Saccharomyces cerevisiae. Genetics 139: 1521–1532.
Kaminsky, R., C. Denison, U. Bening-Abu-Shach, A. D. Chisholm, S. P. Gygi *et al.*, 2009 SUMO regulates the assembly and function of a cytoplasmic intermediate filament protein in C. elegans. Dev. Cell 17: 724–735.
Katic, I., L. Xu, and R. Ciosk, 2015 CRISPR/Cas9 genome gediting in Caenorhabditis elegans: evaluation of templates for homology-mediated hmrepair and knock-kins by homology-hindependent DNA repair. G3 5: 1649–1656.
Keeney, S., C. N. Giroux, and N. Kleckner, 1997 Meiosis-specific DNA double-strand breaks are catalyzed by Spo11, a member of a widely conserved protein family. Cell 88: 375–384.
Kim, H. M., and M. P. Colaiacovo, 2014 ZTF-8 interacts with the 9-1-1 complex and is required for DNA damage response and double-strand break repair in the C. elegans germline. PLoS Genet. 10: e1004723.
Kim, H. M., and M. P. Colaiacovo, 2015 DNA damage sensitivity dsassays in Caenorhabditis elegans. Bio Protoc. 5: e1487.

Kim, S. H., and W. M. Michael, 2008 Regulated proteolysis of DNA polymerase eta during the DNA-damage response in C. elegans. Mol. Cell 32: 757–766.
Klapholz, S., C. S. Waddell, and R. E. Esposito, 1985 The role of the SPO11 gene in meiotic recombination in yeast. Genetics 110: 187–216.
Klug, H., M. Xaver, V. K. Chaugule, S. Koidl, G. Mittler *et al.*, 2013 Ubc9 sumoylation controls SUMO chain formation and meiotic synapsis in Saccharomyces cerevisiae. Mol. Cell 50: 625–636.
Kovalenko, O. V., A. W. Plug, T. Haaf, D. K. Gonda, T. Ashley *et al.*, 1996 Mammalian ubiquitin-conjugating enzyme Ubc9 interacts with Rad51 recombination protein and localizes in synaptonemal complexes. Proc. Natl. Acad. Sci. USA 93: 2958–2963.
Kurtzman, A. L., and N. Schechter, 2001 Ubc9 interacts with a nuclear localization signal and mediates nuclear localization of the paired-like homeobox protein Vsx-1 independent of SUMO-1 modification. Proc. Natl. Acad. Sci. USA 98: 5602–5607.
Lapenta, V., P. Chiurazzi, P. van der Spek, A. Pizzuti, F. Hanaoka *et al.*, 1997 SMT3A, a human homologue of the S. cerevisiae SMT3 gene, maps to chromosome 21qter and defines a novel gene family. Genomics 40: 362–366.
Lawrie, N. M., C. Tease, and M. A. Hulten, 1995 Chiasma frequency, distribution and interference maps of mouse autosomes. Chromosoma 104: 308–314.
Lee, J. H., and T. T. Paull, 2005 ATM activation by DNA double-strand breaks through the Mre11-Rad50-Nbs1 complex. Science 308: 551–554.
Leight, E. R., D. Glossip, and K. Kornfeld, 2005 Sumoylation of LIN-1 promotes transcriptional repression and inhibition of vulval cell fates. Development 132: 1047–1056.
Li, Y., Q. Zhang, Q. Wei, Y. Zhang, K. Ling *et al.*, 2012 SUMOylation of the small GTPase ARL-13 promotes ciliary targeting of sensory receptors. J. Cell Biol. 199: 589–598.
Lim, Y., D. Lee, K. Kalichamy, S. E. Hong, M. Michalak *et al.*, 2014 Sumoylation regulates ER stress response by modulating calreticulin gene expression in XBP-1-dependent mode in Caenorhabditis elegans. Int. J. Biochem. Cell Biol. 53: 399–408.
Lu, C. S., L. N. Truong, A. Aslanian, L. Z. Shi, Y. Li *et al.*, 2012 The RING finger protein RNF8 ubiquitinates Nbs1 to promote DNA double-strand break repair by homologous recombination. J. Biol. Chem. 287: 43984–43994.
Luo, K., L. Li, Y. Li, C. Wu, Y. Yin *et al.*, 2016 A phosphorylation-deubiquitination cascade regulates the BRCA2-RAD51 axis in homologous recombination. Genes Dev. 30: 2581–2595.
Mahajan, R., C. Delphin, T. Guan, L. Gerace, and F. Melchior, 1997 A small ubiquitin-related polypeptide involved in targeting RanGAP1 to nuclear pore complex protein RanBP2. Cell 88: 97–107.
Malone, R. E., S. Bullard, M. Hermiston, R. Rieger, M. Cool *et al.*, 1991 Isolation of mutants defective in early steps of meiotic recombination in the yeast Saccharomyces cerevisiae. Genetics 128: 79–88.
McKim, K. S., and A. Hayashi-Hagihara, 1998 mei-W68 in Drosophila melanogaster encodes a Spo11 homolog: evidence that the mechanism for initiating meiotic recombination is conserved. Genes Dev. 12: 2932–2942.
Milman, N., E. Higuchi, and G. R. Smith, 2009 Meiotic DNA double-strand break repair requires two nucleases, MRN and Ctp1, to produce a single size class of Rec12 (Spo11)-oligonucleotide complexes. Mol. Cell. Biol. 29: 5998–6005.
Minn, I. L., M. M. Rolls, W. Hanna-Rose, and C. J. Malone, 2009 SUN-1 and ZYG-12, mediators of centrosome-nucleus attachment, are a functional SUN/KASH pair in Caenorhabditis elegans. Mol. Biol. Cell 20: 4586–4595.
Moens, P. B., and B. Spyropoulos, 1995 Immunocytology of chiasmata and chromosomal disjunction at mouse meiosis. Chromosoma 104: 175–182.
Moreau, S., J. R. Ferguson, and L. S. Symington, 1999 The nuclease activity of Mre11 is required for meiosis but not for mating type switching, end joining, or telomere maintenance. Mol. Cell. Biol. 19: 556–566.
Mukai, M., Y. Kitadate, K. Arita, S. Shigenobu, and S. Kobayashi, 2006 Expression of meiotic genes in the germline progenitors of Drosophila embryos. Gene Expr. Patterns 6: 256–266.
Nacerddine, K., F. Lehembre, M. Bhaumik, J. Artus, M. Cohen-Tannoudji *et al.*, 2005 The SUMO pathway is essential for nuclear integrity and chromosome segregation in mice. Dev. Cell 9: 769–779.
Nairz, K., and F. Klein, 1997 mre11S—a yeast mutation that blocks double-strand-break processing and permits nonhomologous synapsis in meiosis. Genes Dev. 11: 2272–2290.
Nimonkar, A. V., J. Genschel, E. Kinoshita, P. Polaczek, J. L. Campbell *et al.*, 2011 BLM-DNA2-RPA-MRN and EXO1-BLM-RPA-MRN constitute two DNA end resection machineries for human DNA break repair. Genes Dev. 25: 350–362.
Novak, J. E., P. B. Ross-Macdonald, and G. S. Roeder, 2001 The budding yeast Msh4 protein functions in chromosome synapsis and the regulation of crossover distribution. Genetics 158: 1013–1025.
Nowak, M., and M. Hammerschmidt, 2006 Ubc9 regulates mitosis and cell survival during zebrafish development. Mol. Biol. Cell 17: 5324–5336.
Olson, E., C. J. Nievera, E. Liu, A. Y. Lee, L. Chen *et al.*, 2007 The Mre11 complex mediates the S-phase checkpoint through an interaction with replication protein A. Mol. Cell. Biol. 27: 6053–6067.
Ouyang, K. J., M. K. Yagle, M. J. Matunis, and N. A. Ellis, 2013 BLM SUMOylation regulates ssDNA accumulation at stalled replication forks. Front. Genet. 4: 167.
Paix, A., Y. Wang, H. E. Smith, C. Y. Lee, D. Calidas *et al.*, 2014 Scalable and versatile genome editing using linear DNAs with microhomology to Cas9 sites in Caenorhabditis elegans. Genetics 198: 1347–1356.
Paquis-Flucklinger, V., S. Santucci-Darmanin, R. Paul, A. Saunieres, C. Turc-Carel *et al.*, 1997 Cloning and expression analysis of a meiosis-specific MutS homolog: the human MSH4 gene. Genomics 44: 188–194.
Parameswaran, B., H. C. Chiang, Y. Lu, J. Coates, C. X. Deng *et al.*, 2015 Damage-induced BRCA1 phosphorylation by Chk2 contributes to the timing of end resection. Cell Cycle 14: 437–448.
Paull, T. T., and M. Gellert, 1999 Nbs1 potentiates ATP-driven DNA unwinding and endonuclease cleavage by the Mre11/Rad50 complex. Genes Dev. 13: 1276–1288.
Pawlowski, W. P., I. N. Golubovskaya, and W. Z. Cande, 2003 Altered nuclear distribution of recombination protein RAD51 in maize mutants suggests the involvement of RAD51 in meiotic homology recognition. Plant Cell 15: 1807–1816.
Pelisch, F., and R. T. Hay, 2016 Tools to study SUMO conjugation in Caenorhabditis elegans. Methods Mol. Biol. 1475: 233–256.
Pelisch, F., R. Sonneville, E. Pourkarimi, A. Agostinho, J. J. Blow *et al.*, 2014 Dynamic SUMO modification regulates mitotic chromosome assembly and cell cycle progression in Caenorhabditis elegans. Nat. Commun. 5: 5485.
Pelisch, F., T. Tammsalu, B. Wang, E. G. Jaffray, A. Gartner *et al.*, 2017 A SUMO-dependent protein network regulates chromosome dpnrccongression during oocyte omeiosis. Mol. Cell 65: 66–77.
Penkner, A., L. Tang, M. Novatchkova, M. Ladurner, A. Fridkin *et al.*, 2007 The nuclear envelope protein Matefin/SUN-1 is required for homologous pairing in C. elegans meiosis. Dev. Cell 12: 873–885.

Pfander, B., G. L. Moldovan, M. Sacher, C. Hoege, and S. Jentsch, 2005 SUMO-modified PCNA recruits Srs2 to prevent recombination during S phase. Nature 436: 428–433.

Pferdehirt, R. R., and B. J. Meyer, 2013 SUMOylation is essential for sex-specific assembly and function of the Caenorhabditis elegans dosage compensation complex on X chromosomes. Proc. Natl. Acad. Sci. USA 110: E3810–E3819.

Plug, A. W., A. H. Peters, K. S. Keegan, M. F. Hoekstra, P. de Boer *et al.*, 1998 Changes in protein composition of meiotic nodules during mammalian meiosis. J. Cell Sci. 111: 413–423.

Porter, S. E., and J. J. Champoux, 1989 The basis for camptothecin enhancement of DNA breakage by eukaryotic topoisomerase I. Nucleic Acids Res. 17: 8521–8532.

Poukka, H., P. Aarnisalo, U. Karvonen, J. J. Palvimo, and O. A. Janne, 1999 Ubc9 interacts with the androgen receptor and activates receptor-dependent transcription. J. Biol. Chem. 274: 19441–19446.

Prelich, G., M. Kostura, D. R. Marshak, M. B. Mathews, and B. Stillman, 1987 The cell-cycle regulated proliferating cell nuclear antigen is required for SV40 DNA replication in vitro. Nature 326: 471–475.

Qiao, H., H. B. Prasada Rao, Y. Yang, J. H. Fong, J. M. Cloutier *et al.*, 2014 Antagonistic roles of ubiquitin ligase HEI10 and SUMO ligase RNF212 regulate meiotic recombination. Nat. Genet. 46: 194–199.

Raderschall, E., A. Bazarov, J. Cao, R. Lurz, A. Smith *et al.*, 2002 Formation of higher-order nuclear Rad51 structures is functionally linked to p21 expression and protection from DNA damage-induced apoptosis. J. Cell Sci. 115: 153–164.

Ragland, R. L., S. Patel, R. S. Rivard, K. Smith, A. A. Peters *et al.*, 2013 RNF4 and PLK1 are required for replication fork collapse in ATR-deficient cells. Genes Dev. 27: 2259–2273.

Rao, H. B., H. Qiao, S. K. Bhatt, L. R. Bailey, H. D. Tran *et al.*, 2017 A SUMO-ubiquitin relay recruits proteasomes to chromosome axes to regulate meiotic recombination. Science 355: 403–407.

Rasmussen, S. W., and P. B. Holm, 1984 The synaptonemal complex, recombination nodules and chiasmata in human spermatocytes. Symp. Soc. Exp. Biol. 38: 271–292.

Reynolds, A., H. Qiao, Y. Yang, J. K. Chen, N. Jackson *et al.*, 2013 RNF212 is a dosage-sensitive regulator of crossing-over during mammalian meiosis. Nat. Genet. 45: 269–278.

Robison, J. G., J. Elliott, K. Dixon, and G. G. Oakley, 2004 Replication protein A and the Mre11.Rad50.Nbs1 complex co-localize and interact at sites of stalled replication forks. J. Biol. Chem. 279: 34802–34810.

Rojas-Fernandez, A., A. Plechanovova, N. Hattersley, E. Jaffray, M. H. Tatham *et al.*, 2014 SUMO chain-induced dimerization activates RNF4. Mol. Cell 53: 880–892.

Rojowska, A., K. Lammens, F. U. Seifert, C. Direnberger, H. Feldmann *et al.*, 2014 Structure of the Rad50 DNA double-strand break repair protein in complex with DNA. EMBO J. 33: 2847–2859.

Romanienko, P. J., and R. D. Camerini-Otero, 1999 Cloning, characterization, and localization of mouse and human SPO11. Genomics 61: 156–169.

Roy Chowdhuri, S., T. Crum, A. Woollard, S. Aslam, and P. G. Okkema, 2006 The T-box factor TBX-2 and the SUMO conjugating enzyme UBC-9 are required for ABa-derived pharyngeal muscle in C. elegans. Dev. Biol. 295: 664–677.

Sacher, M., B. Pfander, C. Hoege, and S. Jentsch, 2006 Control of Rad52 recombination activity by double-strand break-induced SUMO modification. Nat. Cell Biol. 8: 1284–1290.

Sarangi, P., R. Steinacher, V. Altmannova, Q. Fu, T. T. Paull *et al.*, 2015 Sumoylation influences DNA break repair partly by increasing the solubility of a conserved end resection protein. PLoS Genet. 11: e1004899.

Seeber, A., A. M. Hegnauer, N. Hustedt, I. Deshpande, J. Poli *et al.*, 2016 RPA mediates recruitment of MRX to forks and double-strand dbreaks to hold sister chromatids together. Mol. Cell 64: 951–966.

Shim, E. Y., W. H. Chung, M. L. Nicolette, Y. Zhang, M. Davis *et al.*, 2010 Saccharomyces cerevisiae Mre11/Rad50/Xrs2 and Ku proteins regulate association of Exo1 and Dna2 with DNA breaks. EMBO J. 29: 3370–3380.

Shinohara, A., H. Ogawa, and T. Ogawa, 1992 Rad51 protein involved in repair and recombination in S. cerevisiae is a RecA-like protein. Cell 69: 457–470.

Silva, S., V. Altmannova, N. Eckert-Boulet, P. Kolesar, I. Gallina *et al.*, 2016 SUMOylation of Rad52-Rad59 synergistically change the outcome of mitotic recombination. DNA Repair (Amst.) 42: 11–25.

Skilton, A., J. C. Ho, B. Mercer, E. Outwin, and F. Z. Watts, 2009 SUMO chain formation is required for response to replication arrest in S. pombe. PLoS One 4: e6750.

Snowden, T., S. Acharya, C. Butz, M. Berardini, and R. Fishel, 2004 hMSH4-hMSH5 recognizes holliday hjunctions and forms a meiosis-specific sliding clamp that embraces homologous chromosomes. Mol. Cell 15: 437–451.

Song, J., L. K. Durrin, T. A. Wilkinson, T. G. Krontiris, and Y. Chen, 2004 Identification of a SUMO-binding motif that recognizes SUMO-modified proteins. Proc. Natl. Acad. Sci. USA 101: 14373–14378.

Su, H. L., and S. S. Li, 2002 Molecular features of human ubiquitin-like SUMO genes and their encoded proteins. Gene 296: 65–73.

Swan, K. A., D. E. Curtis, K. B. McKusick, A. V. Voinov, F. A. Mapa *et al.*, 2002 High-throughput gene mapping in Caenorhabditis elegans. Genome Res. 12: 1100–1105.

Takahashi, Y., S. Dulev, X. Liu, N. J. Hiller, X. Zhao *et al.*, 2008 Cooperation of sumoylated chromosomal proteins in rDNA maintenance. PLoS Genet. 4: e1000215.

Takanami, T., S. Sato, T. Ishihara, I. Katsura, H. Takahashi *et al.*, 1998 Characterization of a Caenorhabditis elegans recA-like gene Ce-rdh-1 involved in meiotic recombination. DNA Res. 5: 373–377.

Tanaka, K., J. Nishide, K. Okazaki, H. Kato, O. Niwa *et al.*, 1999 Characterization of a fission yeast SUMO-1 homologue, pmt3p, required for multiple nuclear events, including the control of telomere length and chromosome segregation. Mol. Cell. Biol. 19: 8660–8672.

Tatham, M. H., E. Jaffray, O. A. Vaughan, J. M. Desterro, C. H. Botting *et al.*, 2001 Polymeric chains of SUMO-2 and SUMO-3 are conjugated to protein substrates by SAE1/SAE2 and Ubc9. J. Biol. Chem. 276: 35368–35374.

Tomimatsu, N., B. Mukherjee, J. L. Harris, F. L. Boffo, M. C. Hardebeck *et al.*, 2017 DNA-damage-induced degradation of EXO1 exonuclease limits DNA end resection to ensure accurate DNA repair. J. Biol. Chem. 292: 10779–10790.

Tsur, A., U. Bening Abu-Shach, and L. Broday, 2015 ULP-2 SUMO protease regulates E-cadherin recruitment to adherens junctions. Dev. Cell 35: 63–77.

Tzur, Y. B., A. Margalit, N. Melamed-Book, and Y. Gruenbaum, 2006 Matefin/SUN-1 is a nuclear envelope receptor for CED-4 during Caenorhabditis elegans apoptosis. Proc. Natl. Acad. Sci. USA 103: 13397–13402.

Usui, T., T. Ohta, H. Oshiumi, J. Tomizawa, H. Ogawa *et al.*, 1998 Complex formation and functional versatility of Mre11 of budding yeast in recombination. Cell 95: 705–716.

van der Linden, E., H. Sanchez, E. Kinoshita, R. Kanaar, and C. Wyman, 2009 RAD50 and NBS1 form a stable complex functional in DNA binding and tethering. Nucleic Acids Res. 37: 1580–1588.

Voelkel-Meiman, K., L. F. Taylor, P. Mukherjee, N. Humphryes, H. Tsubouchi *et al.*, 2013 SUMO localizes to the central element of synaptonemal complex and is required for the full synapsis of meiotic chromosomes in budding yeast. PLoS Genet. 9: e1003837.

Vyas, R., R. Kumar, F. Clermont, A. Helfricht, P. Kalev *et al.*, 2013 RNF4 is required for DNA double-strand break repair in vivo. Cell Death Differ. 20: 490–502.

Walker, M. Y., and R. S. Hawley, 2000 Hanging on to your homolog: the roles of pairing, synapsis and recombination in the maintenance of homolog adhesion. Chromosoma 109: 3–9.

Ward, J. D., N. Bojanala, T. Bernal, K. Ashrafi, M. Asahina *et al.*, 2013 Sumoylated NHR-25/NR5A regulates cell fate during C. elegans vulval development. PLoS Genet. 9: e1003992.

Wicks, S. R., R. T. Yeh, W. R. Gish, R. H. Waterston, and R. H. Plasterk, 2001 Rapid gene mapping in Caenorhabditis elegans using a high density polymorphism map. Nat. Genet. 28: 160–164.

Williams, R. S., J. S. Williams, and J. A. Tainer, 2007 Mre11-Rad50-Nbs1 is a keystone complex connecting DNA repair machinery, double-strand break signaling, and the chromatin template. Biochem. Cell Biol. 85: 509–520.

Williams, R. S., G. E. Dodson, O. Limbo, Y. Yamada, J. S. Williams *et al.*, 2009 Nbs1 flexibly tethers Ctp1 and Mre11-Rad50 to coordinate DNA double-strand break processing and repair. Cell 139: 87–99.

Windecker, H., and H. D. Ulrich, 2008 Architecture and assembly of poly-SUMO chains on PCNA in Saccharomyces cerevisiae. J. Mol. Biol. 376: 221–231.

Wu, C. S., and L. Zou, 2016 The SUMO (small subiquitin-like modifier) ligase PIAS3 primes ATR for checkpoint activation. J. Biol. Chem. 291: 279–290.

Yin, Y., and S. Smolikove, 2013 Impaired resection of meiotic double-strand breaks channels repair to nonhomologous end joining in Caenorhabditis elegans. Mol. Cell. Biol. 33: 2732–2747.

Yin, Y., A. Seifert, J. S. Chua, J. F. Maure, F. Golebiowski *et al.*, 2012 SUMO-targeted ubiquitin E3 ligase RNF4 is required for the response of human cells to DNA damage. Genes Dev. 26: 1196–1208.

Yin, Y., S. Donlevy, and S. Smolikove, 2016 Coordination of recombination with meiotic progression in the Caenorhabditis elegans germline by KIN-18, a TAO kinase that regulates the timing of MPK-1 signaling. Genetics 202: 45–59.

Yokoo, R., K. A. Zawadzki, K. Nabeshima, M. Drake, S. Arur *et al.*, 2012 COSA-1 reveals robust homeostasis and separable licensing and reinforcement steps governing meiotic crossovers. Cell 149: 75–87.

Yoshida, K., G. Kondoh, Y. Matsuda, T. Habu, Y. Nishimune *et al.*, 1998 The mouse RecA-like gene Dmc1 is required for homologous chromosome synapsis during meiosis. Mol. Cell 1: 707–718.

Youds, J. L., D. G. Mets, M. J. McIlwraith, J. S. Martin, J. D. Ward *et al.*, 2010 RTEL-1 enforces meiotic crossover interference and homeostasis. Science 327: 1254–1258.

Yunus, A. A., and C. D. Lima, 2009 Structure of the Siz/PIAS SUMO E3 ligase Siz1 and determinants required for SUMO modification of PCNA. Mol. Cell 35: 669–682.

Zheng, L., R. Kanagaraj, B. Mihaljevic, S. Schwendener, A. A. Sartori *et al.*, 2009 MRE11 complex links RECQ5 helicase to sites of DNA damage. Nucleic Acids Res. 37: 2645–2657.

Communicating editor: J. Engebrecht